



# Membrane cholesterol regulates TRPV4 function, cytoskeletal expression, and the cellular response to tension

Monika Lakk<sup>1</sup>, Grace F. Hoffmann<sup>1</sup>, Aruna Gorusupudi<sup>1</sup>, Eric Enyong<sup>2</sup>, Amy Lin<sup>1</sup>, Paul S. Bernstein<sup>1</sup>, Trine Toft-Bertelsen<sup>3</sup>, Nanna MacAulay<sup>3</sup>, Michael H. Elliott<sup>2</sup>, and David Križaj<sup>1,4,5\*</sup>

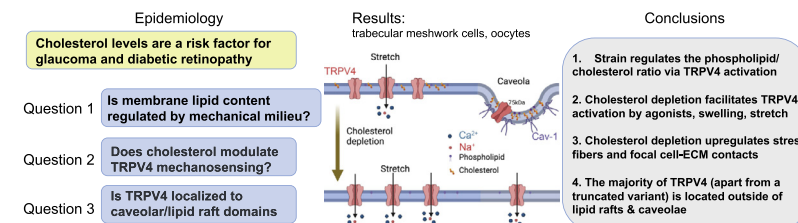
<sup>1</sup>Department of Ophthalmology & Visual Sciences, University of Utah School of Medicine, Salt Lake City, UT, USA; <sup>2</sup>Dean A. McGee Eye Institute, University of Oklahoma Health Sciences Center, Oklahoma City, OK, USA; <sup>3</sup>Department of Neuroscience, University of Copenhagen, Copenhagen, Denmark; <sup>4</sup>Department of Bioengineering, and <sup>5</sup>Department of Neurobiology, University of Utah, Salt Lake City, UT, USA

**Abstract** Despite the association of cholesterol with debilitating pressure-related diseases such as glaucoma, heart disease, and diabetes, its role in mechanotransduction is not well understood. We investigated the relationship between mechanical strain, free membrane cholesterol, actin cytoskeleton, and the stretch-activated transient receptor potential vanilloid isoform 4 (TRPV4) channel in

human trabecular meshwork (TM) cells. Physiological levels of cyclic stretch resulted in time-dependent decreases in membrane cholesterol/phosphatidylcholine ratio and upregulation of stress fibers. Depleting free membrane cholesterol with m-β-cyclodextrin (MβCD) augmented TRPV4 activation by the agonist GSK1016790A, swelling and strain, with the effects reversed by cholesterol supplementation. MβCD increased membrane expression of TRPV4, caveolin-1, and flotillin. TRPV4 did not colocalize or interact with caveolae or lipid rafts, apart from a truncated ~75 kDa variant partially precipitated by a caveolin-1 antibody. MβCD induced currents in TRPV4-expressing *Xenopus laevis* oocytes. Thus, membrane cholesterol regulates trabecular transduction of mechanical information, with TRPV4 channels mainly located outside the cholesterol-enriched membrane domains. Moreover, the biomechanical milieu itself shapes the lipid content of TM membranes. Diet, cholesterol metabolism, and mechanical stress might modulate the conventional outflow pathway and intraocular pressure in glaucoma and diabetes in part by modulating TM mechanosensing.

**Supplementary key words** cell signaling • cyclodextrins • dyslipidemias • eye/retina • glaucoma • lipid rafts • mechanotransduction • smooth muscle cells • TRPV4

Conversion of sensory information into electrical and chemical signals in eukaryotic cells is modulated by unesterified cholesterol, a planar 27-carbon polycyclic molecule that constitutes ~20% of the total mass of membrane lipids (1, 2). Its intercalation into phospholipids reduces the motion of hydrocarbon chains, affects surface charge, and promotes membrane stiffness while keeping the membrane fluid (3–5). Cholesterol is a precursor for steroid hormones and regulates stereospecific interactions with transmembrane channels, transporters, and enzymes within membrane-bound glycosphingolipid-rich protein complexes (lipid rafts;



(6)) that serve as organizing hubs for intracellular signaling pathways, membrane trafficking, cytoskeleton, and cell-extracellular matrix (ECM) interactions (1, 2, 7, 8). Alterations in free membrane cholesterol and lipid raft density positively and negatively affect membrane channels, with little consensus about the molecular mechanisms (9–11).

Vertebrates maintain cholesterol levels within a narrow range, with deficits or oversupply often harmful for health (5, 6). Defects in cholesterol regulation contribute to atherosclerosis, myocardial injury, diabetic and vascular dysfunctions (12–14), and increase the risk for progression of neurodegenerative diseases such as primary open-angle glaucoma, a prevalent cause of blindness (15, 16). Patients with high serum cholesterol levels have an increased likelihood for elevated intraocular pressure (IOP), with glaucoma linked to multiple genes involved in cholesterol metabolism (17, 18). A

\*For correspondence: David Križaj, [david.krizaj@hsc.utah.edu](mailto:david.krizaj@hsc.utah.edu).



principal regulator of IOP is the trabecular meshwork (TM), a multilayered tissue composed of smooth muscle-like cells with mechanosensitive and contractile functions (16, 19–21). In response to mechanical stress and glaucoma, TM cells upregulate actomyosin cytoskeleton, ECM secretion, and the size/number of focal cell-ECM contacts, thereby increasing cell contractility and tissue resistance to the outflow of aqueous humor (22–25). It is not known how TM membrane lipid composition is affected by the biomechanical milieu and whether changes in membrane stiffness impelled by free membrane cholesterol affect TM mechanosensing, intracellular signaling, and cytoskeletal organization.

We recently identified the mechanosensitive transient receptor potential vanilloid 4 (TRPV4) channel as a principal regulator of mechanically induced signaling in mouse and human TM (20, 26, 27). This ubiquitous nonselective cation channel transduces the effects of membrane strain, shear flow, swelling, and thermal stimuli into calcium signals, which control a wide range of downstream signaling pathways (21, 26, 28, 29). The TRPV4 sequence appears to have coevolved with enzymes linked to cholesterol biosynthesis pathways (30). Studies in endothelial cells suggested that TRPV4 is trafficked to cholesterol- and caveolin-1 (Cav-1)-enriched rafts (31) to modulate vascular flow (32) but the interactions between mechanotransduction, TRPV4 signaling, and cholesterol are not well understood. We used human TM cells and an oocyte overexpression system to investigate cholesterol-dependent modulation of TRPV4 signaling in model mammalian and non-mammalian systems. Interestingly, phosphatidylcholine (PC) versus cholesterol content of TM membranes was regulated by stretch in a TRPV4-dependent manner. TRPV4 was mainly located in nonraft regions, as indicated by the lack of interaction and absence of colocalization with caveolar and noncaveolar components of lipid rafts. Lowering the levels of free membrane cholesterol facilitated TRPV4 activation and promoted cytoskeletal polymerization. These findings suggest a potential mechanism whereby diet, the biomechanical milieu, and systemic/local cholesterol homeostatically regulate the aqueous outflow pathway.

## MATERIALS AND METHODS

### TM cell culture and isolation

Primary cultures of TM cells were dissected from three eyes of donors with no history of eye disease (65-year-old male, 68-year-old male, and 78-year-old male) as described previously (26, 27, 33) and in concordance with the tenets of the World Medical Association Declaration of Helsinki and the Department of Health and Human Services Belmont Report. A subset of experiments was conducted in immortalized juxtaganular human TM cells obtained from ScienCell (catalog no. 6590) and used up to the seventh passage. Primary and immortalized human TM cells showed no

differences in responses to TRPV4 or cholesterol-modulating agents. Cells were grown in trabecular meshwork cell medium (TMCM; ScienCell; catalog no. 6591) at 37°C and 5% CO<sub>2</sub>. The phenotype was periodically validated by profiling for markers, including *Aqp1*, *Timp3*, *Myoc*, *MGP*, *Acta2* ( $\alpha$ -smooth muscle actin [ $\alpha$ SMA]), and dexamethasone-induced upregulation of myocilin expression. These data are shown in our previous characterizations of the cell line (21, 26, 33).

*Xenopus laevis* oocyte experiments were performed according to the guidelines of the Danish Veterinary and Food Administration (Ministry of Environment and Food) and approved by the animal facility at the Faculty of Health and Medical Sciences, University of Copenhagen. The experiments conform to the principles and regulations described (34). The surgical protocol by which the oocytes were retrieved was approved by The Danish National Committee for Animal Studies, Danish Veterinary and Food Administration (Ministry of Environment and Food). This work appeared previously in abstract and preprint forms (35, 36).

### Reagents

The TRPV4 agonist GSK1016790A (GSK101) and cholesterol were obtained from Sigma or VWR. GSK101 (1 mM) stock aliquots were prepared in dimethyl sulfoxide and subsequently diluted into working saline concentrations (5 and 25 nM, respectively). Chemical reagents for biochemical experiments—methanol, isopropanol, *n*-hexane, and chloroform—were of GC/MS grade and purchased from Thermo Fisher Scientific. The cholesterol standard was purchased from Sigma-Aldrich.

### Cholesterol depletion and repletion

Methyl- $\beta$ -cyclodextrin (M $\beta$ CD; Sigma; C4555) was dissolved in TMCM and used at 10 mM, the concentration that removes 80–90% of free membrane cholesterol (37, 38). Cells were preincubated with M $\beta$ CD for 60 min to maximize extraction, washed in TMCM, and placed into recording chambers for optical recordings. This protocol maintains decreased membrane cholesterol levels for at least 24 h (39). Supplementation was based on perfusion with cholesterol-saturated M $\beta$ CD. Powdered cholesterol was dissolved for 30 min in 80% ethanol solution at 75–80°C to obtain a 10 mM stock solution. The stock was dissolved in TMCM containing M $\beta$ CD to the final cholesterol concentration of 1 mM. A parallel chamber used the cholesterol stock to load M $\beta$ CD for the final concentrations of 1 mM cholesterol + 10 mM M $\beta$ CD.

### Hypotonic stimulation

The swelling studies were conducted as reported previously (40, 41). Extracellular NaCl was kept at 57.5 mM, and total osmolarity was regulated by adding or removing mannitol, a procedure that maintains the ionic strength of the extracellular solution. Osmolarity was checked thermometrically using a vapor pressure osmometer (Wescor).

### Lipid extraction and GC/MS chromatography

Lipids were extracted using Folch method (42). Total lipids were extracted by adding methanol/chloroform/water (1:2:1, v/v). The chloroform phase was washed to remove water residues and dried under nitrogen gas. The dried film was dissolved in 100  $\mu$ l hexane, and 5  $\mu$ l of the sample was injected into the GC/MS instrument for cholesterol analysis. The

Thermo Trace GC-DSQ II system (Thermo Fisher Scientific) consists of an automatic sample injector (AS 3000), gas chromatograph, single quadrupole mass detector, and an analytical workstation. Chromatographic separation was carried out with an Rx-5MS-coated 5% diphenyl/95% dimethyl polysiloxane capillary column (30 m × 0.25 mm inner diameter, 0.25 µm film thickness) (Restek Corporation, PA). The sample was injected into the GC/MS using a splitless mode, the septum purge was on, and the injector temperature was set at 200°C. The column temperature was programmed as follows: initial temperature 60°C, 15°/min to 240°C, 2°/min to 290°C, and a hold at 290°C for 5 min. Transfer line temperature was 290°C. Helium was used as the carrier gas at a flow rate of 1.5 ml/min. MS conditions were as follows: electron ionization mode with ion source temperature of 250°C and multiplier voltage, 1,182 V; full scan and selected ion monitoring mode was used to identify and quantify cholesterol. The area values of cholesterol were plotted against known range of standards (100–0.1 ng) to quantify the cholesterol in the samples. PC levels were measured by a colorimetric/fluorometric assay kit (BioVision).

### Immunoprecipitation and Western blot analysis

Cell lysis was performed in lysis buffer containing 2% octylglucoside, 150 mM NaCl, 10 mM Tris-HCl, pH 7.4, 0.5 mM EDTA, 0.1% Triton X-100, and protease inhibitor cocktail (Roche). Lysates were cleared by centrifugation, and protein concentrations determined using a BCA assay (Thermo Fisher Scientific). Immunoprecipitation of Cav-1 was performed using Dynabeads™ Protein G Kit (Thermo Fisher Scientific) according to the manufacturer's instructions. Briefly, Cav-1 primary antibody (10 ng/µl) was conjugated to Dynabeads magnetic beads at room temperature. Then, an equal amount of protein from each sample was incubated with the beads-antibody conjugates for 15 min at room temperature, with gentle agitation. The beads were removed from solution by DynaMag™-2 magnet (Thermo Fisher Scientific), washed in wash buffer, and resuspended in lysis buffer. The original cell lysates, immunoprecipitates, and unbound fractions (flow-through) were boiled in Laemmli buffer, separated by reducing SDS-PAGE and transferred to nitrocellulose membranes. Membranes were blocked with 5% BSA for 1 h, and probed with Cav-1 (Cell Signaling Technology) and TRPV4 primary antibodies (Alomone Lab). Primary antibodies were detected using Clean-Blot® IP detection reagent (Thermo Fisher Scientific) conjugated to HRP.

### Detergent-free lipid raft isolation and Western blot analysis

Samples were homogenized in hypotonic homogenization buffer (20 mM Tris-HCl, pH 7.8, 3 mM MgCl<sub>2</sub>, 10 mM NaCl, 0.0005 mg/ml, 2 mM sodium vanadate, 20 mM sodium fluoride, 0.5 mM DTT, and 1 mM PMSF) on ice and centrifuged at 15,000 g for 30 min at 4°C to separate cytosolic proteins from intracellular and plasma membranes. The pellet was resuspended in 0.5 M Na<sub>2</sub>CO<sub>3</sub>, transferred to a 5%/35%/45% sucrose (in Na<sub>2</sub>CO<sub>3</sub>) flotation gradient and spun at 36,000 rpm for 18 h using a preparative ultracentrifuge model XL-90 (NVT90 rotor; Beckman Coulter Life Sciences). Fractions obtained from the sucrose gradient were diluted in hypotonic buffer and spun at 15,000 g for 30 min at 4°C. Pellets (25 µl) were resuspended in RIPA buffer and 2× Laemmli buffer. About 30 µl of each sample was loaded in 10% SDS-PAGE and transferred to PVDF membranes for 1 h at 220 mA.

Nonspecific binding was blocked with 5% nonfat milk and 2% BSA. The samples were incubated overnight at 4°C with TRPV4 (1:500; Alomone Labs), flotillin (1:200; Santa Cruz Biotechnology), Cav-1 (1:1,000; Cell Signaling), and α-SMA (1:500; Sigma-Aldrich) antibodies, followed by anti-mouse (1:5,000; BioRad) or anti-rabbit (1:5,000; Cell Signaling) HRP-conjugated secondary antibodies. The blotted proteins were developed with an enhanced chemiluminescence kit (Thermo Fisher Scientific).

### Immunofluorescence

Cells were fixed with 4% paraformaldehyde for 10 min. After a phosphate-buffered saline (PBS) rinse, PBS containing 5% FBS and 0.3% Triton X-100 blocking solution was applied for 20 min. Filamentous actin (F-actin) was labeled with AlexaFluor 488 phalloidin (1:1,000; Life Technologies). Primary antibodies (rabbit anti-TRPV4, 1:1,000, Lifespan Biosciences; mouse antiflotillin, 1:200, Santa Cruz; and mouse anticaveolin, 1:1,000, BD Biosciences) were diluted in antibody solution (2% BSA and 0.2% Triton X-100 in PBS) and applied overnight at 4°C. The TRPV4 antibody does not label TRPV4 KO tissues (43, 44). After rinsing, slices were incubated with secondary antibodies diluted to 1:1,000 in PBS for 1 h at room temperature. Plasma membrane cholesterol was tracked with filipin (Sigma; F9765). As previously described (45), 0.005% filipin (Sigma) was dissolved in dimethyl sulfoxide and applied to dissociated cells together with the secondary antibody (goat anti-rabbit AlexaFluor 488; 1:500; Life Technologies). Unbound antibodies were rinsed, and conjugated fluorophores were protected with Fluoromount-G (Southern Biotech) prior to coverslipping. Images (10 per experiment) were acquired on Olympus CV1200 confocal microscope using a NeoFluor 20× water immersion objective.

### Analysis and particle counting

Images were acquired using identical parameters (HV, gain, and offset), resulting in very similar signal-to-noise ratios across datasets. ImageJ (National Institutes of Health) was used to extract and quantify the mean intensities and particle analysis of immunoreactive signals, with ~40–50 cells per slide averaged across at least three independent experiments. The fluorescence intensity of F-actin was measured in arbitrary units using the area integrated intensity measurement tool of ImageJ with background compensation. Data were plotted as the signal as averaged and normalized fluorescence intensity (in percent) per cell area compared with the control. In particle analysis, color images were converted to black and white using *Binary* → *Convert to mask* with white background and automatic threshold level. Immunoreactive puncta (number/cell area) with the segmented area were counted with the *Analyze particles* plug-in. Minimum (3 pixel<sup>2</sup>) and maximum (30 pixel<sup>2</sup>) pixel area sizes were defined to exclude regions outside the regions of interest (ROIs), calculate the particle number/cell area, and determine the relative puncta numbers. Individual particle sizes for each cell were averaged and normalized.

### Optical imaging

Calcium responses in TM cells were tracked following published protocols (43, 46, 47). Briefly, for charge-coupled device imaging, cells were loaded with 5–10 µM Fura-2-AM for 45 min and perfused with isotonic saline (pH 7.4) containing (in millimolar): NaCl 133, KCl 2.5, NaH<sub>2</sub>PO<sub>4</sub> 1.5, MgCl<sub>2</sub>

( $6\text{H}_2\text{O}$ ) 1.5,  $\text{CaCl}_2$  2, glucose 10, HEPES hemisodium salt 10, pyruvic acid 1, lactic acid 1, L-glutamine 0.5, glutathione 0.5, sodium ascorbate 0.3, with pH 7.4, and osmolarity at  $300 \pm 10$  mOsm, delivered through a gravity-fed 8-reservoir system (Warner Instruments) that converged toward a manifolds tube inserted into the experimental chamber. Epifluorescence was detected with Photometrics Delta or Prime BSI cameras. Ratiometric  $\text{Ca}^{2+}$  imaging was performed on ROIs that marked a central somatic region and were typically binned at  $3 \times 3$  (43, 46). Background fluorescence was measured in similarly sized TM ROIs in neighboring areas devoid of cells. The microscopes were inverted with a Nikon Ti with  $40\times$  (0.75 numerical aperture [NA] oil) or upright Nikon E600 FN microscopes with a  $20\times$  (0.8 NA water) and  $40\times$  (1.3 NA oil and 0.8 NA water) objectives. A wide-spectrum 150 W Xenon arc lamp (DG4; Sutter Instruments, Novato, CA) provided excitation to 340 and 380 nm filters (Semrock). The signals were analyzed using NIS-Elements Advanced Research 3.2 and MS. Excel  $\Delta R/R$  (peak  $F^{340}/F^{380}$  ratio – baseline/baseline) was used to quantify the amplitude of  $\text{Ca}^{2+}$  signals. Data acquisition and  $F^{340}/F^{380}$  ratio calculations were performed by NIS Elements 3.22 software (Melville, NY).

## Spectrophotometry

The intracellular calcium concentration [ $\text{Ca}^{2+}$ ]<sub>i</sub> was monitored using a plate reader (Turner Biosystems). Cells were seeded onto noncoated 96-well plates and loaded with 2  $\mu\text{M}$  of Fluo-4 AM for 30–45 min at 37°C. Fluorescence was measured at an excitation of 490 nm and an emission of 520 nm, with intervals of 90 s and 6–10 measurements per experiment. About 490/520 nm ratios were normalized to the control untreated samples. Baseline measurements were recorded in control wells at the same time without addition of agonist or hypotonic stimuli (HTS).

## Membrane strain assay

TM cells were seeded on flexible silicon membranes coated with type I/IV collagen, grown to 80% confluence, and placed into a FlexJunior chamber controlled by the Flexcell-5000 Tension system (Flexcell) (26). Stretch-induced  $\text{Ca}^{2+}$  influx and cytoskeletal changes were tracked in cells loaded with Fura-2-AM for 30–60 min and stimulated with cyclic biaxial stretch (10%, 1 Hz, 15 min, or 6%, 0.5 Hz 1–3 h, respectively) at 37°C. Changes in focal plane (which disrupted calcium

imaging for several seconds, as indicated by breaks in response trace in Fig. 1A) were adjusted manually. Cells were imaged with a Nikon E600FN upright microscope. Excitation light was provided by a Xenon source within a Lambda DG4 (Sutter Instruments) and controlled by Nikon Elements.

## RNA preparation and heterologous expression in *Xenopus laevis* oocytes

*Xenopus laevis* frogs were obtained from Nasco (Fort Atkinson). The frogs were kept in tanks in a recirculating water facility and fed twice weekly with Floating Frog Food 3/32 for adults and juveniles (Xenopus Express, Inc). Oocytes were surgically removed from anesthetized frogs (41, 48) under anesthesia (2 g/l tricain, 3-aminobenzoic acid ethyl ester; Sigma A-5040). Preparation of defolliculated oocytes was carried out as described (49). Oocytes were kept in Kuller medium (in millimolar): 90 NaCl, 1 KCl, 1  $\text{CaCl}_2$ , 1  $\text{MgCl}_2$ , 5 HEPES (pH 7.4). Complementary DNA encoding rat TRPV4 was subcloned into the oocyte expression vector pXOOM, linearized downstream from the poly-A segment, and in vitro transcribed using T7 mMessage machine according to the manufacturer's instructions (Ambion). Complementary RNA was extracted with MEGAclear (Ambion) and microinjected into defolliculated *Xenopus laevis* oocytes: 4 ng TRPV4 RNA/oocyte. A TRP channel antagonist, ruthenium red (1  $\mu\text{M}$ ; Sigma-Aldrich; R-2751), was added to the medium to prevent tonic TRPV4-mediated currents mediating oocyte lysis. The oocytes were kept for 3–4 days at 19°C before experiments.

## Electrophysiology on *Xenopus laevis* oocytes

Conventional two-electrode voltage-clamp studies were performed with a DAGAN CA-1B High-Performance oocyte clamp (DAGAN) with Digidata 1440A interface controlled by pCLAMP software, version 10.5 (Molecular Devices). Electrodes were pulled (HEKA and PIP5) from borosilicate glass capillaries to a resistance of 2.5–3  $\text{M}\Omega$  when filled with 1 M KCl. The current traces were obtained in a test solution containing (in millimolar): 50 NaCl, 2 KCl, 1  $\text{MgCl}_2$ , 1  $\text{CaCl}_2$ , 10 HEPES, 100 mM mannitol (Tris-buffered pH 7.4, 220 mOsm) by stepping the clamp potential from -20 mV to test potentials ranging from +50 to -130 mV (pulses of 200 ms) in increments of 15 mV. Recordings were low pass filtered at 500 Hz, sampled at 1 kHz, and steady-state current activity analyzed at 140–180 ms after applying the test pulse. Depletion

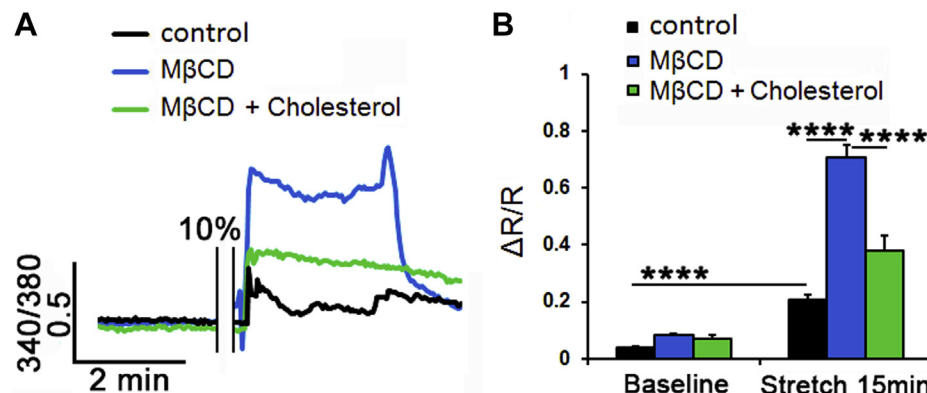


**Fig. 1.** Membrane cholesterol modulates the cyclic stretch-induced intracellular calcium responses in TM cells. A: Representative traces. B: Averaged results for 15 min cyclic stretch of control (black trace, bars), M $\beta$ CD-treated (10 mM, blue trace, bar), and M $\beta$ CD:cholesterol-treated (green trace, bar) TM cells. Stretch-evoked [ $\text{Ca}^{2+}$ ]<sub>i</sub> responses are modulated by membrane cholesterol ( $n = 21\text{--}77$ ;  $N = 5\text{--}6$ ). \*\*\* $P < 0.0001$ .

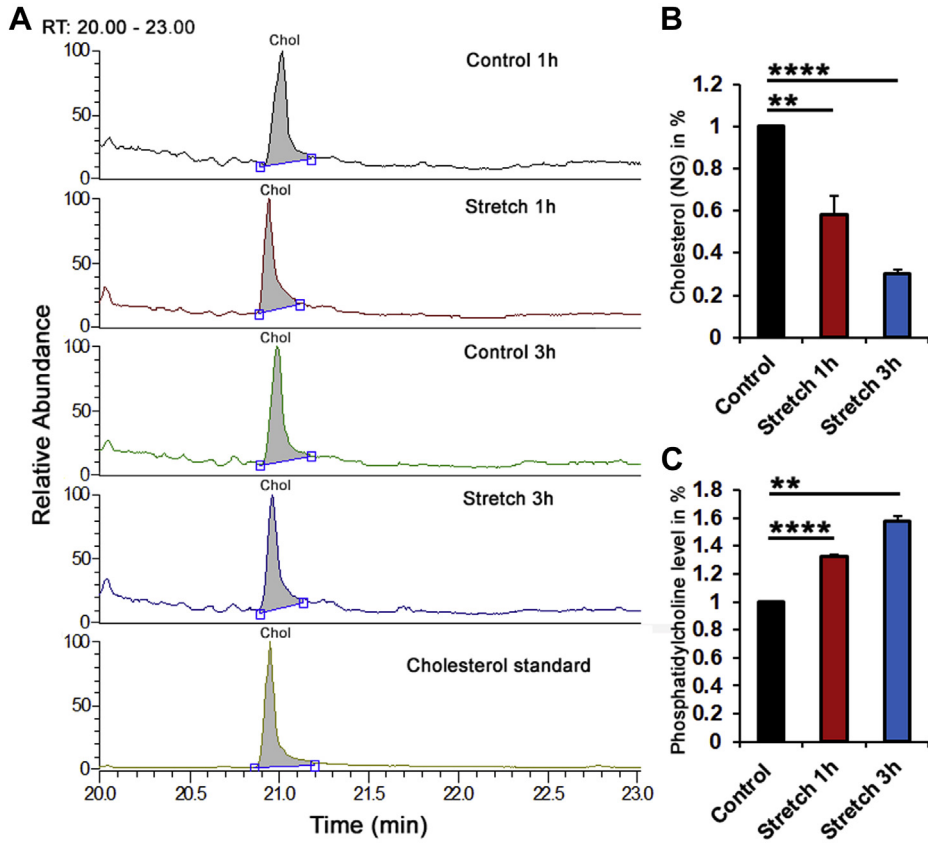


**Fig. 2.** The C/P ratio in TM membranes is stretch dependent. A: Representative chromatograms. B: Normalized and averaged cholesterol GS/MS data in control, 1 and 3 h stretched primary TM cells. C: Normalized and averaged PC fluorometric data in control, 1 and 3 h stretched primary TM cells. Stretch induced a time-dependent decrease in membrane cholesterol level, which was concomitant with increasing content of PC membrane. N = 3; \*\*P < 0.01; \*\*\*P < 0.0001.

of endogenous cholesterol in intact oocytes was induced with 50  $\mu$ M M $\beta$ CD for 45 min (e.g., 55). All experiments were performed at room temperature (23°C).

### Data analysis

Statistical analyses were performed with GraphPad Prism 6.0 (GraphPad) and Origin Pro 8.5 (OriginLab). Data were acquired from at least three different experimental preparations on different days, with 3–6 slides/experiment. Typically three different batches of oocytes were used. Unless indicated otherwise, unpaired or paired *t*-tests were used to compare two means, and a one-way ANOVA along with the Tukey test was used to compare three or more means. Means are shown  $\pm$  SEM. P > 0.05 = not significant; P < 0.05 = \*, P < 0.01 = \*\*, P < 0.001 = \*\*\*, and P < 0.0001 = \*\*\*\*. Preliminary versions of this study were published in abstract (35) and preprint (36) forms.

## RESULTS

### The cholesterol/phosphatidylcholine ratio of the TM membrane is regulated by tensile stretch

The mechanical properties of the lipid bilayer can change under tension (50), but it is not known whether the biomechanical milieu shapes the membrane lipid content. To test this, we assessed changes in cholesterol

content and the C/PC (cholesterol/PC) molar ratio following the stimulation of cells with cyclic mechanical strain. Primary human TM cells were isolated from healthy donors (26, 27), plated on ECM (collagen I)-coated membranes, and stimulated for 1 or 3 h with radial stretch (0.5 Hz; 6% elongation). Membrane C/PC levels were measured with GS/MS and a fluorometric PC assay. Normalized relative to unstimulated controls, the stretched samples showed time-dependent decrease in membrane cholesterol content to  $0.58 \pm 0.089$  (1 h; N = 3; P < 0.01) and  $0.30 \pm 0.02$  (3 h; N = 3; P < 0.001) (Fig. 2A, B), whereas the PC content increased to  $1.32 \pm 0.02$  (1 h; N = 3; P < 0.0001) and  $1.58 \pm 0.03$  (3 h; N = 3; P < 0.01), respectively (Fig. 2C). The membrane C/PC ratio (control, C/PC = 1) decreased to 0.44 following 1 h and 0.19 after 3 h of mechanical stimulation. Its sensitivity to the mechanical strain suggests that mechanical properties of the cell membrane reflect the history of exposure to the biomechanical environment.

### Reduction in free membrane cholesterol results in lipid raft loss

Membrane cholesterol was modulated with M $\beta$ CD, a water-soluble cyclic oligosaccharide that encapsulates hydrophobic membrane cholesterol residues and has

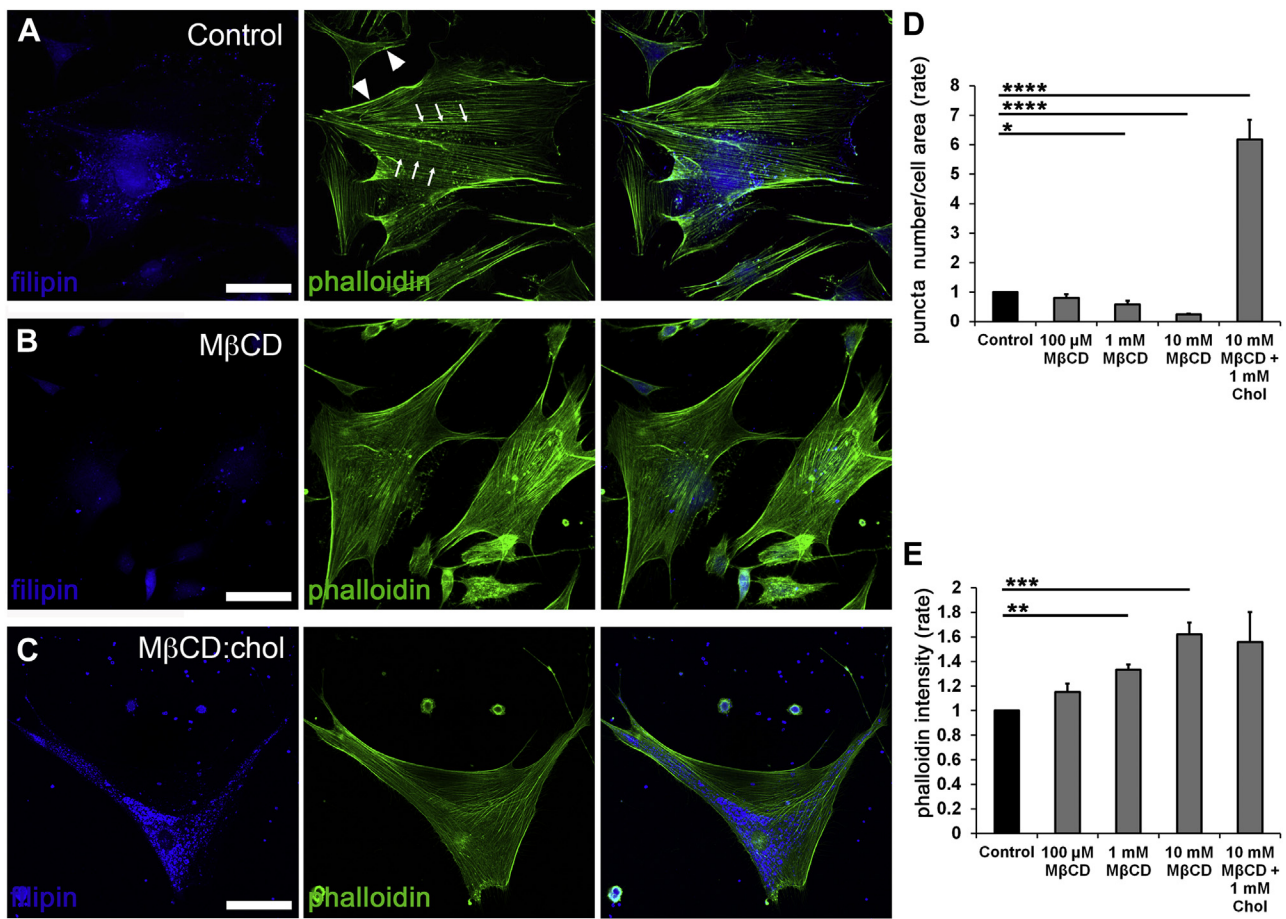


**Fig. 3.** Cholesterol depletion promotes formation of actin stress fibers. Double labeling for F-actin (phalloidin-Alexa 488 nm) and filipin (405 nm). A: Untreated preparations show typical stress fiber organization dotted by lipid rafts. B: About 1 h of incubation with M<sub>β</sub>CD results in dissolution of filipin<sup>+</sup> puncta and upregulation of phalloidin-actin fluorescence. C: Saturated 1:10 admixture of cholesterol (1 mM) and M<sub>β</sub>CD (10 mM) increased the number of filipin puncta. D, E: Averaged data for experiments shown in A–C ( $N = 3–4$ ). \* $P < 0.05$ , \*\* $P < 0.01$ , \*\*\* $P < 0.001$ , and \*\*\*\* $P < 0.0001$ . The scale bar represents 20  $\mu$ m.

been widely used to characterize cholesterol dependence of ion channels (37). Endogenous unesterified cholesterol within lipid rafts was visualized with filipin, a fluorescent polyene antibiotic (51, 52). About 60 min of incubation with M<sub>β</sub>CD (10 mM) reduced filipin-positive puncta by  $75.63\% \pm 2.77\%$  ( $P < 0.0001$ ) (Fig. 3A, B, and D), with cells remaining viable and responsive to physiological stimuli throughout a typical experiment (~1–3 h). Cholesterol:M<sub>β</sub>CD supplementation (1:10) (38) increased the number of filipin-positive puncta by  $6.17 \pm 0.67$ -fold (Fig. 3C, D). These data show that formation of raft domains in TM cells is predicated upon free membrane cholesterol levels.

#### Reduction in free membrane cholesterol is associated with upregulated expression of F-actin

Mechanical stability and structural integrity of cells are maintained by cortical actin (arrowheads in Fig. 3A) and ventral stress fibers (arrows), which are often reinforced in response to mechanical stress (19, 24, 27). We tested whether altering membrane stiffness through cholesterol depletion/enrichment impacts

cytoskeletal architecture in cells labeled with phalloidin-actin Alexa 488. One-hour exposure to 0.1–10 mM M<sub>β</sub>CD was associated with dose-dependent increases in stress fiber fluorescence. Exposure to 10 mM cyclodextrin increased the F-actin signal by  $55.8 \pm 9.5\%$  (Fig. 3B, E) ( $N = 4$ ;  $P < 0.001$ ), whereas supplementation with saturated 1:10 (1 mM) mixture of cholesterol and M<sub>β</sub>CD did not affect actin expression (Fig. 3C, E) despite the sizeable increase in the number of filipin<sup>+</sup> puncta (Fig. 3C, D). Thus, actomyosin organization in TM cells does not appear to require lipid rafts.

#### Cholesterol depletion facilitates agonist-induced TRPV4 activation

TRPV4, a polymodal calcium-permeable channel that recently emerged as potential regulator of TM pressure, strain and volume sensing, and conventional outflow (20, 26, 27) contains putative cholesterol recognition motifs within Loop4-TM5 (30). Its sensitivity to cholesterol modulation was investigated in cells loaded with the Ca<sup>2+</sup> indicator dye Fura-2-AM and

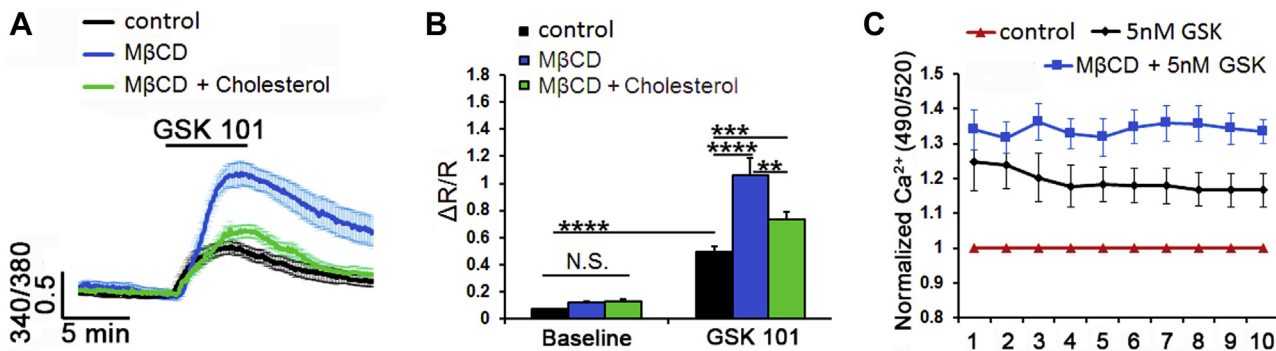


**Fig. 4.** Cholesterol depletion increases the amplitude of TRPV4 agonist-induced  $\text{Ca}^{2+}$  signals. A, B: Ratiometric signals in Fura-2 AM-loaded cells. A: GSK101-induced elevations are increased in M $\beta$ CD-treated cells ( $n = 8\text{--}10$ ). B: Averaged data. M $\beta$ CD (blue bar) augmented, whereas M $\beta$ CD:cholesterol (green bar) reduced the amplitude of agonist-induced fluorescence. C: Fluorimetry, cell populations in 96 wells. About 5 nM GSK101 increased Fluo-4 fluorescence. Its effect was facilitated (~12%) by M $\beta$ CD ( $N = 4$ ). \*\*\* $P < 0.01$ ; \*\*\*\* $P < 0.001$ ; NS, nonsignificant.

stimulated with the agonist GSK1016780A (GSK101) before and after exposure to M $\beta$ CD. As previously shown (26, 27), GSK101 (25 nM) reversibly increased  $[\text{Ca}^{2+}]_{\text{TM}}$  (Fig. 4A). M $\beta$ CD increased the peak amplitude of the GSK101-evoked signal from  $0.5 \pm 0.04$  ( $n = 39$ ;  $N = 6$ ) to  $1.06 \pm 0.13$  ( $n = 53$ ;  $N = 6$ ;  $P < 0.0001$ ) (Fig. 4A, B) (~100% increase) without affecting baseline  $[\text{Ca}^{2+}]_{\text{i}}$ . Agonist stimulation under cholesterol-enriched conditions produced a small but significant increase in the average GSK101 response ( $0.74 \pm 0.05$ ;  $n = 44$ ;  $N = 5$ ;  $P < 0.001$ ) (Fig. 4A, B).

Spectrophotometry was used to assess the effects of cholesterol depletion on the TM population response. About 5 nM GSK101 produced a  $24.8 \pm 8.31\%$  increase in the Fluo-4 fluorescence signal ( $N = 4$  independent experiments;  $P < 0.05$ ; supplemental Fig. S1A). M $\beta$ CD potentiated the response by ~12%, resulting in  $36.27 \pm 5.18\%$  increase compared with the baseline ( $P < 0.05$ ) (Fig. 4C). A similar facilitatory effect was observed with 25 nM GSK101 (supplemental Fig. S1A). These data suggest that cholesterol suppresses agonist-induced TRPV4 activation.

### Cholesterol modulates swelling-induced calcium signaling

Originally identified as a regulator of cellular swelling (53, 54), TRPV4 functions as a real-time readout of cell volume changes (48) with osmoregulatory functions in neurons, glia, epithelial, and endothelial cells (40, 41, 55–58). To determine the effect of raft disruption on the TM swelling response, we exposed the cells to HTS in the presence/absence of M $\beta$ CD. Consistent with TRPV4 activation, TM cells responded to 140 mOsm HTS with significant ( $0.44 \pm 0.06$ ;  $n = 24$ ;  $N = 4$ ;  $P < 0.0001$ ) increases in  $[\text{Ca}^{2+}]_{\text{i}}$  (Fig. 5A, B). Depletion of cholesterol doubled the peak response amplitude to  $0.87 \pm 0.08$  ( $n = 27$ ;  $N = 4$ ;  $P < 0.001$ ), with the facilitatory effect inhibited by cholesterol supplementation ( $0.43 \pm 0.04$ ;  $n = 30$ ;  $N = 4$ ;  $P < 0.001$ ) (Fig. 5A, B). Spectrophotometry similarly showed dose-dependent  $[\text{Ca}^{2+}]_{\text{i}}$  increases in response to HTS (in case of 55% HTS:  $1.14 \pm 0.03$ ;  $N = 3$ ) and augmentation by cholesterol removal (to  $1.21 \pm 0.022$ ;  $N = 3$ ) (Fig. 5C and supplemental Fig. S1B) ( $P < 0.05$ ).

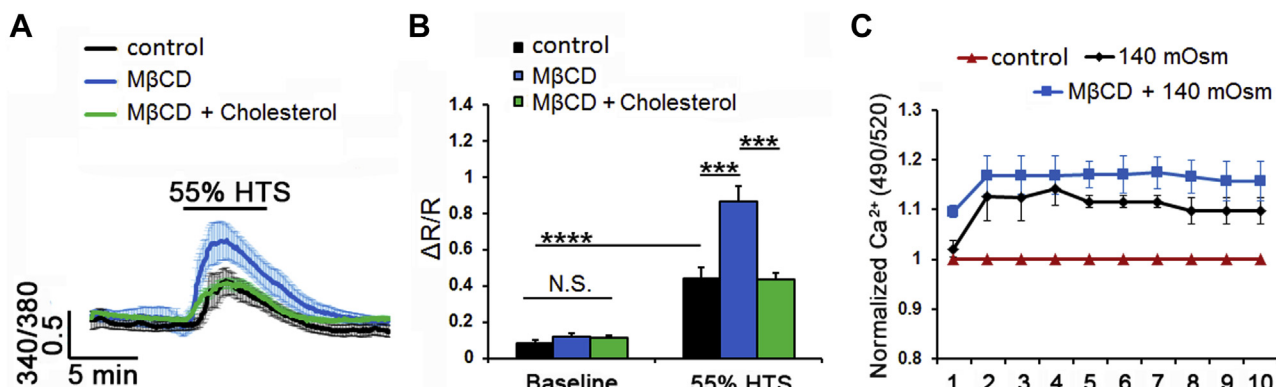


**Fig. 5.** Cholesterol depletion facilitates HTS-induced  $\text{Ca}^{2+}$  signals. A, B: Cytosolic  $\text{Ca}^{2+}$  responses in Fura-2 AM-loaded cells. A: HTS induced  $[\text{Ca}^{2+}]_{\text{i}}$  elevations in representative control, M $\beta$ CD and M $\beta$ CD:cholesterol-treated samples ( $n = 8\text{--}10$ ). B: Averaged data from A. M $\beta$ CD (blue bar) augmented, whereas M $\beta$ CD:cholesterol (green bar) reduced HTS-induced  $[\text{Ca}^{2+}]_{\text{i}}$  increases. C: Fluorimetry. 55% HTS (140 mOsm) increased Fluo-4 signals. This effect was facilitated by M $\beta$ CD ( $N = 3$ ). \*\*\* $P < 0.001$ ; \*\*\*\* $P < 0.0001$ ; NS, nonsignificant.

## Cholesterol modulates the TM response to membrane strain

We next investigated whether cholesterol depletion impacts the transduction of cyclic mechanical stretch, which mirrored strains impelled on ECM beams by IOP fluctuations (59–61) that are transduced partly via TRPV4 (20, 27). Cells were stimulated with periodic and calibrated displacements/relaxations of the collagen IV-coated substrate (1 Hz; 10% elongation, 15 min). In response to stretch, cytosolic  $[Ca^{2+}]_i$  reversibly increased to  $0.21 \pm 0.02$  ( $n = 21$ ;  $N = 6$ ;  $P < 0.0001$ ) (Fig. 1A, B). The effect was augmented by cholesterol depletion to  $0.71 \pm 0.04$  ( $n = 77$ ;  $N = 5$ ;  $P < 0.0001$ ) and reduced by cholesterol supplementation to  $0.38 \pm 0.05$  ( $n = 37$ ;  $N = 6$ ;  $P < 0.0001$ ) (Fig. 1A, B). Simvastatin (10  $\mu$ M), an inhibitor of 3-hydroxy-3-methylglutaryl coenzyme A reductase, the rate-limiting endogenous enzyme in cholesterol biosynthesis, induced a small and nonsignificant decrease in the number of filipin<sup>+</sup> puncta (supplemental Fig. S2A, B). Accordingly, the statin did not affect the amplitude or kinetics of stress-induced  $[Ca^{2+}]_i$  elevations ( $0.16 \pm 0.01$ ;  $n = 12$ ;  $N = 2$ ) (supplemental Fig. S2C, D).

Changes in membrane cholesterol content have been shown to influence cell surface tension and actomyosin assembly (62). To test the effect of membrane cholesterol on stress fibers, F-actin was labeled with fluorescent phalloidin following exposure to cyclic stretch in the presence/absence of MβCD and MβCD:cholesterol. As shown previously, stretch alone augmented phalloidin-actin fluorescence (to  $1.32 \pm 0.05$ ;  $N = 3$ ;  $P < 0.001$ ) (Fig. 6A, C). Interestingly, this was associated with a significant decrease in the density of filipin puncta (to  $0.76 \pm 0.05$ ;  $N = 3$ ;  $P < 0.01$ ) (Fig. 6A, B), suggesting that mechanical stress influences the formation of lipid rafts. As shown in Fig. 3, MβCD increased the F-actin signal ( $1.56 \pm 0.09$ ;  $N = 3$ ;  $P < 0.0001$ ) while reducing filipin fluorescence to  $0.24 \pm 0.03$  ( $N = 3$ ;  $P < 0.0001$ ). MβCD treatment of stretch-exposed cells did not further affect filipin fluorescence ( $0.26 \pm 0.02$ ;  $N = 3$ ) (Fig. 6A, B), whereas stress fiber fluorescence showed a significant  $42.6\% \pm 21.6\%$  increase over the effect of stretch alone ( $N = 3$ ;  $P < 0.05$ ) (Fig. 6C). These data suggest that stretch and cholesterol depletion facilitate F-actin expression in an additive manner and that stretch functions as a negative regulator of raft assembly.

## Membrane cholesterol regulates TRPV4 expression

Depending on the cell type and protein isoform, cholesterol-modulating agents potentiate or inhibit TRP channel trafficking (63–65). We tested how free membrane cholesterol impacts TRPV4 channel expression in fixed cells labeled with a validated antibody (40, 42). One-hour incubation with MβCD produced a  $4.49 \pm 1.07$ -fold increase in the number of TRPV4-ir (immunoreactivity [ir]) puncta ( $N = 3$ ;  $P < 0.05$ ) (Fig. 7 A, B, D). Cholesterol enrichment abrogated this effect ( $0.73 \pm 0.28$ ;  $N = 3$ ;  $P < 0.05$ ) (Fig. 7C, D).

## MβCD potentiates TRPV4 current in heterologously expressing oocytes

The opening of the TRPV4 channel pore in mammalian cells reflects many simultaneous inputs, including mechanical stressors, temperature, polyunsaturated fatty acids, and accessory binding proteins (58, 66, 67). To isolate the effects of cholesterol on the channel from auxiliary proteins and intracellular signaling within TM cells, we determined the cholesterol dependence of TRPV4 currents in the *Xenopus laevis* expression system that has been used in previous studies of cholesterol depletion (68) and TRPV4 signaling (40, 41, 48). Because oocyte viability is compromised at millimolar MβCD concentrations (68), the experiments were conducted using 50  $\mu$ M MβCD.

Membrane currents in uninjected control oocytes and TRPV4-expressing *Xenopus* oocytes were monitored by standard two-electrode voltage clamp. A voltage step protocol demonstrated small tonic currents in TRPV4-expressing oocytes (Fig. 8A, upper left panel) compared with those obtained in uninjected oocytes (Fig. 8A, lower left panel), summarized in Fig. 8B and inset,  $N = 9$ . Transmembrane currents of uninjected oocytes were undisturbed by MβCD exposure, whereas those of the TRPV4-expressing oocytes were enhanced approximately 10-fold (from  $156 \pm 42$  to  $1,466 \pm 475$  nA,  $N = 9$ ,  $P = 0.014$ ) by cholesterol depletion (Fig. 8A [right panels], B). These data indicate that membrane cholesterol suppresses tonic TRPV4 activity, with insufficiency thereof enhancing the TRPV4-mediated membrane currents.

## TRPV4 is predominantly outside the caveolae/lipid rafts

To determine whether TRPV4 is enriched in lipid rafts, detergent-free lipids were isolated by gradient (5%/35%/45% sucrose) ultracentrifugation, and fractions were analyzed by Western blot. Flotillin-1, Cav-1, and α-SMA antibodies were used as markers for noncaveolar lipid, caveolar lipid, and cytosolic fractions, respectively. The 48 kDa noncaveolar lipid raft marker flotillin-1 labeled fractions 3–6. The caveolar marker Cav-1 (~22 kDa) predominantly labeled fractions 3–6, with weak signal present in fractions 1 and 2, whereas α-SMA (~42 kDa) was confined to the supernatant/cytosol fraction. The TRPV4 protein mainly partitioned into the flotillin-free fraction 2, which showed a weak Cav-1 signal (Fig. 9A). Thus, by far the main fraction of membrane TRPV4 is located in nonraft domains that lack caveolar and noncaveolar markers. It is possible that a limited amount of Cav-1 protein shares the membrane with TRPV4 in fraction 2 (Fig. 9A), without direct interaction between the proteins (Fig. 9B, C).

TRPV4 in cultured endothelial cells coimmunoprecipitates with Cav-1 (31, 32). To test the interaction in TM cells, Cav-1 was immunoprecipitated from TM cell lysates, and association with TRPV4 was assessed by

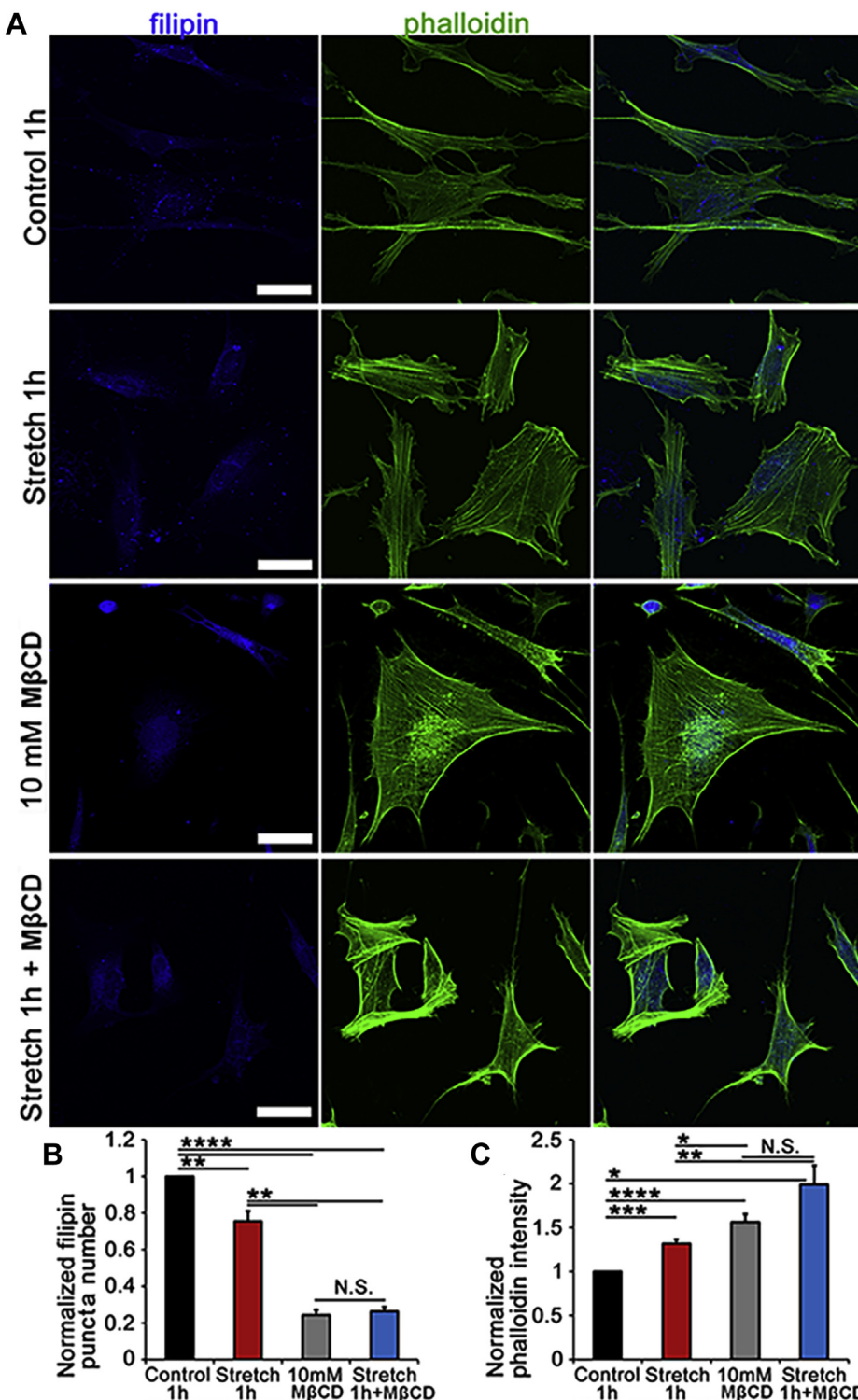


**Fig. 6.** Membrane cholesterol content regulates stretch dependence of cytoskeletal remodeling. A: TM cells were stretched in the presence/absence of M $\beta$ CD and M $\beta$ CD:cholesterol and labeled for filipin (405 nm) and phalloidin-Alexa 488 nm in control, 6% stretch (0.5 Hz, 6%, 1 h), M $\beta$ CD and M $\beta$ CD+ stretch samples. B: Averaged and normalized puncta number. Filipin is significantly reduced by stretch and M $\beta$ CD alone. C: Stretch and M $\beta$ CD significantly facilitate F-actin fluorescence. Combined stimulation results in an additional ~30% increase in stress fiber signal ( $N = 3-4$ ). \* $P < 0.05$ ; \*\* $P < 0.01$ ; \*\*\* $P < 0.001$ ; \*\*\*\* $P < 0.0001$ . The scale bar represents 20  $\mu$ m.

Western blotting. The four bands in the Western blot (Fig. 9B) presumably correspond to glycosylated, full-length, and truncated protein (TRPV4A-E, (69–71)). Following quantitative precipitation of Cav-1, a portion of the ~75 kDa truncated variant associated with Cav-1,

whereas all the full-length variants observed in the total lysate partitioned to Cav-1-depleted unbound fractions (Fig. 9D). Thus, the most significant fraction of TRPV4 by far localizes to noncaveolar nonraft membrane domains.

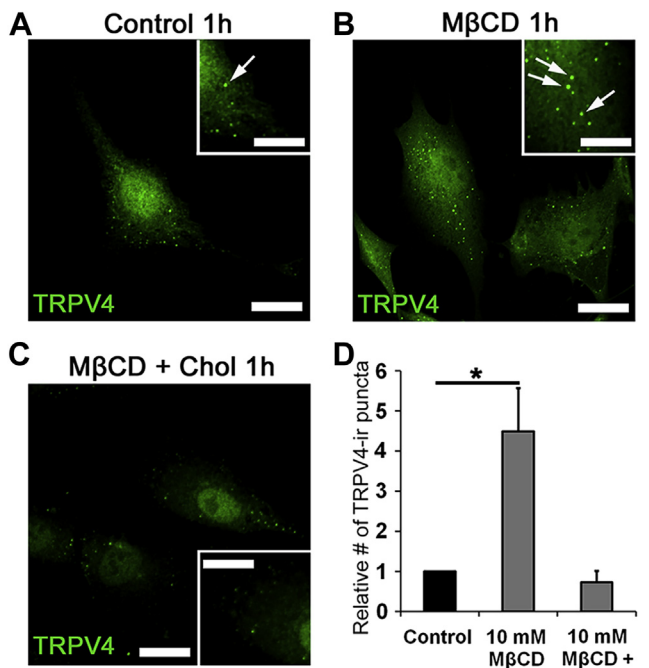


**Fig. 7.** Cholesterol depletion increases the number of TRPV4-ir puncta. TRPV4 immunolabeling of primary TM cells. Representative examples of (A) control, (B) 1 h treatment with MβCD, and (C) 1 h treatment with MβCD+cholesterol. Inset: zoomed-in region with TRPV4-ir puncta (arrow). D: Summary of three independent experiments, normalized for control cells. The number of TRPV4 puncta is upregulated after incubation with MβCD. \*P < 0.05. The scale bar represents 10 μm.

Raft/caveolar localization of TRPV4 was examined further with immunocytochemistry. TRPV4-ir did not colocalize with Cav-1 (Fig. 9C, red arrowheads) and flotillin (Fig. 9D), thereby confirming that TRPV4 does not localize into the raft domains. Cholesterol depletion increased the number of Cav-ir puncta without promoting caveolar TRPV4 translocation.

## DISCUSSION

In this study, we demonstrate that the mechanical milieu regulates the lipid composition of the membrane and that TRPV4, a nonselective cation channel that mediates a wide range of physical and chemical inputs, is highly sensitive to free membrane cholesterol levels. The key findings are *i*) physiological levels of mechanical stretch regulate the TM membrane C/PC ratio, *ii*) the majority of TRPV4 protein is excluded from raft/caveolar regions, with the possible exception of a small proportion of a truncated splice variant that interacts with Cav-1; *iii*) membrane cholesterol negatively modulates TRPV4 activation by agonists and mechanical stimuli; *iv*) TM F-actin expression is cholesterol and stretch dependent; and *v*) cholesterol tonically suppresses TRPV4 activity in a nonmammalian expression system. These findings implicate cholesterol-TRPV4 interactions in dynamic and use-dependent regulation of cellular mechanosensing.

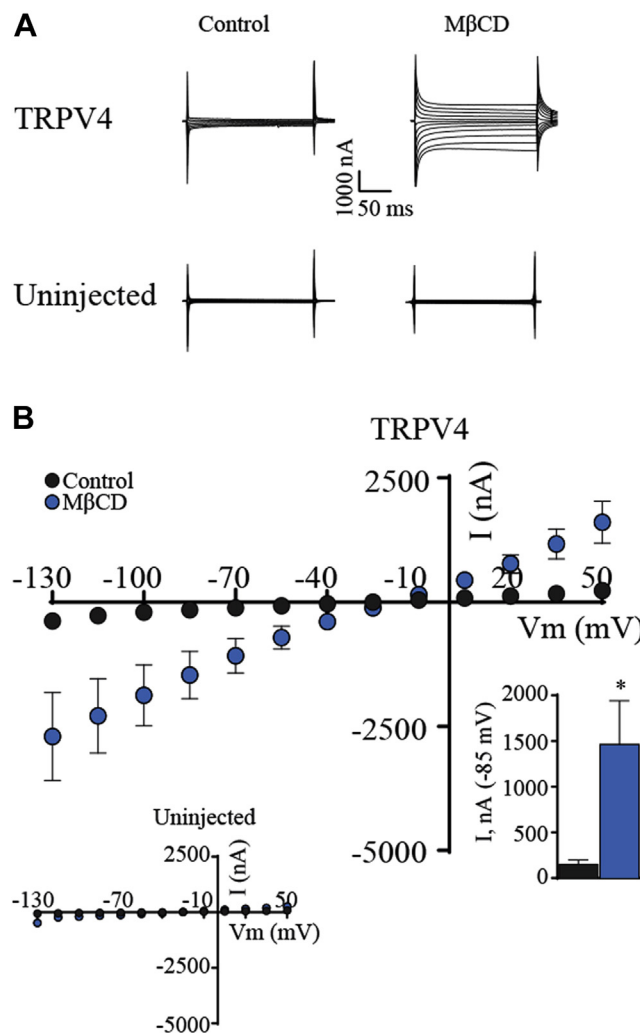


**Fig. 8.** Cholesterol depletion enhances TRPV4-mediated membrane currents in *Xenopus* oocytes. A: Representative current traces from TRPV4-expressing oocytes and uninjected control oocytes in control solution or after 45 min exposure to 50 μM MβCD. B: I/V curves of TRPV4-expressing oocytes exposed to control solution or MβCD, with uninjected oocytes in inset. Summarized currents obtained at -85 mV are shown in the lower inset. The magnitude of TRPV4-mediated currents (at  $V_m = -85$  mV) was compared using Student's t-test. \*\*P < 0.01; N = 9. NS, not significant.

In contrast to the extensive body of knowledge about how lipid composition affects the structural and mechanical properties of biological membranes, much less is known about the relationship between mechanical stress and membrane lipid content. Our finding that cyclic strain lowers the membrane C/PC ratio suggests that biophysical and modulatory properties of biological membranes reflect the biomechanical environment. The sensitivity of stretch-induced reorganization of the lipid content to HC067047 further identifies TRPV4 activation as an obligatory step that couples mechanical strain to lipid signaling. Our second conclusion is that changes in the lipid content may profoundly modulate function of embedded mechanoregulated proteins such as TRPV4. This could be

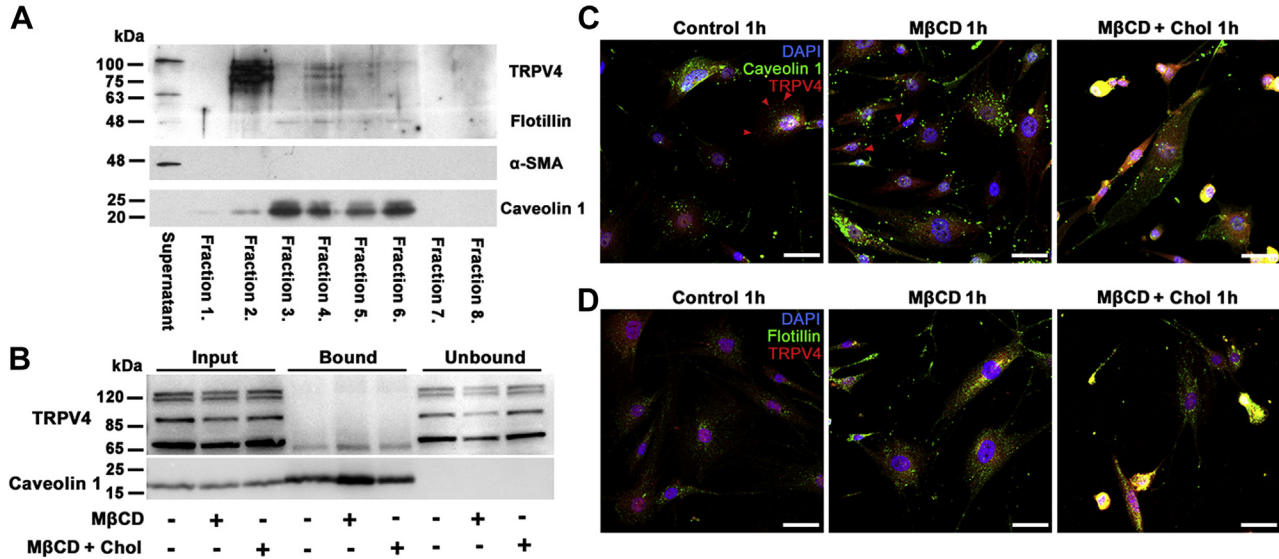


**Fig. 9.** Most membrane TRPV4 does not partition into raft domains or interact with caveolar proteins. **A:** Western blot; detergent-free lipid raft isolation in primary TM cells. The supernatant fraction contains cytosolic proteins; fractions 1 and 2 (5% sucrose) contain nonlipid-raft membrane proteins, fractions 3–6 (5–35% sucrose) contain lipid raft membranes, and fractions 7 and 8 (pellet, 45% sucrose) contain unsuspended proteins and cell nuclei. TRPV4 protein is predominantly confined to fraction 2; fraction 4 is associated with flotillin-1 (48 kDa) and Cav-1 (22 kDa), whereas the supernatant/cytosol fraction associates with α-SMA (42 kDa). **B:** Coimmunoprecipitation. TRPV4-Cav-1 interaction assessed with the Cav-1 antibody for TRPV4 pulldown in control, MβCD, and MβCD:cholesterol-treated samples. Input bands, whole-cell lysate; bound bands, Cav-1-bound protein fraction; unbound bands, flow-through fractions. Cav-1-bound fractions show modest precipitation of the ~75 kDa TRPV4 isoform. The absence of Cav-1 expression in unbound fractions confirms the quantitative immunoprecipitation of Cav-1. **C, D:** Immunohistochemistry, for control, MβCD, and MβCD:cholesterol-treated cells. **C:** Double immunolabeling for TRPV4 and Cav-1. TRPV4-ir (red arrowheads) does not colocalize with Cav-1-ir puncta (green). **D:** Double immunolabeling for TRPV4 and flotillin. TRPV4-ir (red puncta) does not colocalize with flotillin-ir puncta (green). The inset is shown at higher magnification insets as supplemental Fig. S3. The scale bar represents 20 μm.

relevant in blinding diseases such as glaucoma, which has been associated with elevated C/PC ratios in TM cells (22).

Free cholesterol is a central constituent of caveolae and lipid rafts, which serve as regulatory portals for cellular cholesterol homeostasis (1, 2, 5, 7, 72). Its depletion results in near-total dissolution of lipid rafts (visualized by filipin fluorescence) and profoundly modulates Ca<sup>2+</sup> signals induced by the TRPV4 agonist GSK1016790A, cyclic strain, and cell swelling. Given that MβCD similarly facilitates transmembrane currents in TRPV4-expressing, but not control, *X. laevis* oocytes, we propose that the channel is directly and negatively regulated by membrane cholesterol. Supplementation with exogenous MβCD:cholesterol obviated the facilitation induced by the cyclodextrin alone without affecting peak amplitudes of agonist-evoked and mechanically evoked Ca<sup>2+</sup> signals. This may reflect saturation of control membranes with free cholesterol, which constitutes approximately a third of the total membrane lipid mass (5, 38). A similar conclusion was reached for the modulation of the Piezol channel, which is modulated by MβCD but not MβCD:cholesterol (73). The ~4.5-fold increase in the number and intensity of TRPV4-ir puncta (Fig. 7) suggests that cholesterol regulates transport and/or retrieval of TRPV4-containing vesicle pools, as previously shown for

TRPV1 (65, 74), Kvl.5 (75), Kir (39), LRRC8/SWELL (76), and TRPC3 (77) channels. Another possibility is that cholesterol regulates formation of clathrin-coated vesicles (78) and endocytosis/secretion via PACSIN, which binds the N terminus of TRPV4 (75).

Lipids regulate the gating of ion channels through direct interactions within membrane microdomains and indirectly by shaping the biophysical properties of the membrane. An increase in membrane tension, caused by cholesterol removal, might facilitate opening of stretch-activated channels (79, 80) yet viscoelastic “force-from-lipid” models (77, 81, 82) cannot explain why ion channels respond differently to cholesterol enantiomers with similar effects on membrane properties (83). In contrast to its facilitation of TRPV4 signals in TM cells and oocytes, cholesterol depletion suppresses TRPV4 activation in glia (45) and endothelial cells (31). Consistent with allosteric modulation of channel subunits, accessory proteins, and/or residues buried within the bilayer, MβCD facilitates activation of mammalian TRPM8 (63), TRPM3 (64), TRPC3 (77), and volume-activated chloride (76) channels but inhibits TRPA1, TRPC1, TRPC6 (84–86), and blocks TRPL channels in fly photoreceptors (87). Allosteric sites may include cholesterol recognition/interaction amino acid consensus-like (KDLFRFL) recognition motifs that span loop 4-TM5 of TRPV4 (30, 88, 89). Consistent with

our results, loss of TRPV4-cholesterol interaction in the TRPV4<sup>R616Q</sup> inverted cholesterol recognition/interaction amino acid consensus motif mutation was associated with gain of function for TRPV4 (90). Cholesterol thus appears to regulate the context of the cellular sensory response such that TRPV4 activity in yeast (which cannot synthesize cholesterol) responds to swelling but not temperature (91), whereas the mammalian channel is optimally active at ~34–28°C. Similar context dependence was observed in the TRPV1 channel, in which M $\beta$ CD inhibits capsaicin-evoked and proton-evoked currents (92, 93) while facilitating its sensitivity to thermal inputs (92).

Mechanosensing often involves interactions between the cell membrane and the cytoskeleton. Our finding that M $\beta$ CD treatment dissolves lipid rafts and stimulates actin polymerization in TM cells accords with its effects on osteoblasts, fibroblasts, endothelial cells, and myocytes (62, 94, 95). The additivity of the effects of stretch and cholesterol depletion (Fig. 6C) suggests that stretch-activated channels and cholesterol-regulated membrane domains signal via independent mechanisms that converge at the cytoskeleton in order to dynamically regulate membrane/cell stiffness (25–27, 96). In contrast to M $\beta$ CD, simvastatin (which blocks the synthesis of the cholesterol precursor mevalonate) did not affect the amplitude of stretch-induced Ca<sup>2+</sup> signals. Differential effects of simvastatin versus M $\beta$ CD on stress fiber formation and cell contractility have been reported in endothelial cells and fibroblasts (94, 97).

The outflow of aqueous humor is fine tuned by arrays of mechanosensitive molecules that include lipid rafts, caveolae, focal complexes, changes in gene expression, ECM and TRPV4, Piezol, and TREK-1 channels (26, 33, 98–103). TRPV4 in endothelial and smooth muscle cells was reported to interact with Cav-1 (31, 32, 90), and both proteins regulate TM mechanosensitivity and outflow homeostasis (26, 27, 104–106). However, our hypothesis that TM cells manifest TRPV4-Cav-1 interactions in cholesterol-enriched raft/caveolar domains was not confirmed. We found that TRPV4 does not colocalize with filipin (lipid raft marker), Cav-1 (a marker of caveolae), flotillin (marker of noncaveolar rafts), or  $\alpha$ SMA (cytosolic protein marker), and that the majority of the TRPV4 protein, which consists of 871 amino acids with at least five variants with unknown differences in function (70, 71, 107), partitions into fractions that exclude raft proteins. Glycosylated full-length variants (69–71) constitute by far the most significant fraction of the protein and partition into total lysate/unbound fractions that do not contain Cav-1/flotillin and resist cholesterol depletion (Fig. 9D). Interestingly, Cav-1 did precipitate a small portion of the ~75 kDa variant, suggesting that TRPV4 variants might be differentially susceptible to caveolar interaction. Our findings suggest that loss of cholesterol interaction in nonraft regions results in a gain of function for TRPV4 activation (90), as

previously shown for the TRPM8 channel, which shows enhanced gating in nonraft domains (63). It remains to be seen whether TRPV4 variants differ in microdomain interactions with lipids, G-proteins, protein kinases/phosphatases, and/or Ca<sup>2+</sup>-binding proteins.

In summary, our study suggests that TM mechanotransduction is integrated with cholesterol homeostasis. The interdependence between membrane tension, cholesterol content, TRPV4 signaling, and calcium homeostasis suggests that mechanical sensing is a highly dynamic and integrated process that could influence regulation of the conventional outflow pathway. Cholesterol may protect the TM from hypertension-induced injury by downregulating the sensitivity to mechanical stress, but this adaptive function could be compromised by cholesterol dysregulation in glaucoma, diabetic retinopathy, Niemann-Pick disease, and/or macular degeneration.

## Data availability

The data described are contained within the article. 

## Supplemental data

This article contains [supplemental data](#).

## Acknowledgments

The authors thank Dr Peter Geck (Tufts University, Boston, MA) for the generous help with lipid raft experiments. This study was supported by the National Institutes of Health (R01EY027920, R01EY011600, R01EY031817, R01EY028608, P30EY021725, and P30EY014800), Department of Defense–United States Army Medical Research Acquisition Activity (VR200079), ALSAM-Skaggs Foundation, The Neuroscience Initiative at the University of Utah, and an unrestricted grant from Research to Prevent Blindness to Department of Ophthalmology at the University of Utah and the University of Oklahoma Health Sciences Center. The content is solely the responsibility of the authors and does not necessarily represent the official views of the National Institutes of Health.

## Author contributions

M. L. and D. K. conceptualization; M. L., P. S. B., N. M., M. H. E., and D. K. methodology; M. L., A. G., E. E., and T. T.-B. formal analysis; M. L., G. F. H., A. G., E. E., and T. T.-B. investigation; P. S. B., N. M., M. H. E., and D. K. resources; M. L., T. T.-B., N. M., M. H. E., and D. K. writing—original draft; M. L. and D. K. project administration; P. S. B., M. H. E., and D. K. funding acquisition.

## Author ORCIDs

Aruna Gorupupudi  <https://orcid.org/0000-0002-7343-5983>

Eric Enyong  <https://orcid.org/0000-0002-9213-9004>

Amy Lin  <https://orcid.org/0000-0001-9783-1270>

Trine Toft-Bertelsen  <https://orcid.org/0000-0001-9009-0094>

David Križaj  <https://orcid.org/0000-0003-4468-3029>

### Conflict of interest

The authors declare that they have no conflicts of interest with the contents of this article.

### Abbreviations

$\alpha$ SMA,  $\alpha$ -smooth muscle actin;  $[Ca^{2+}]_i$ , intracellular calcium concentration; C/PC, cholesterol/phosphatidylcholine; Cav-1, caveolin-1; ECM, extracellular matrix; F-actin, filamentous actin; HTS, hypotonic stimuli; IOP, intraocular pressure; ir, immunoreactivity; M $\beta$ CD, m- $\beta$ -cyclodextrin; NA, numerical aperture; PBS, phosphate-buffered saline; ROI, region of interest; TM, trabecular meshwork; TMCM, trabecular meshwork cell medium; TRPV4, transient receptor potential vanilloid isoform 4.

Manuscript received December 11, 2020, and in revised from October 8, 2021. Published, JLR Papers in Press, October 25, 2021, <https://doi.org/10.1016/j.jlpr.2021.100145>

### REFERENCES

1. Yeagle, P. L. (1985) Cholesterol, and the cell membrane. *Biochim. Biophys. Acta*. **822**, 267–287
2. Pike, L. J. (2003) Lipid rafts: bringing order to chaos. *J. Lipid Res.* **44**, 655–667
3. Jamieson, G. A., and Robinson, D. M. (1977). *Mammalian Cell Membranes* (vol. 2). Butterworth, London
4. Lundbaek, J. A., Birn, P., Hansen, A. J., Søgaard, R., Nielsen, C., Girshman, J., Bruno, M. J., Tape, S. E., Egebjerg, J., Greathouse, D. V., Mattice, G. L., Koeppel, R. E., and Andersen, O. S. (2004) Regulation of sodium channel function by bilayer elasticity: the importance of hydrophobic coupling. Effects of Micelle-forming amphiphiles and cholesterol. *J. Gen. Physiol.* **123**, 599–621
5. Lange, Y., and Steck, T. L. (2008) Cholesterol homeostasis and the escape tendency (activity) of plasma membrane cholesterol. *Prog. Lipid Res.* **47**, 319–332
6. Subczynski, W. K., Pasenkiewicz-Gierula, M., Widomska, J., Mainali, L., and Raguz, M. (2017) High cholesterol/low cholesterol: effects in biological membranes: a review. *Cell Biochem. Biophys.* **75**, 369–385
7. Sezgin, E., Levental, I., Mayor, S., and Eggeling, C. (2017) The mystery of membrane organization: composition, regulation and roles of lipid rafts. *Nat. Rev. Mol. Cell Biol.* **18**, 361–374
8. Korade, Z., and Kenworthy, A. K. (2008) Lipid rafts, cholesterol, and the brain. *Neuropharmacology* **55**, 1265–1273
9. Mauch, D. H., Nägler, K., Schumacher, S., Göritz, C., Müller, E. C., Otto, A., and Pfrieger, F. W. (2001) CNS synaptogenesis promoted by glia-derived cholesterol. *Science* **294**, 1354–1357
10. Marquer, C., Devauges, V., Cossec, J. C., Liot, G., Lécart, S., Sauvadou, F., Duyckaerts, C., Lévéque-Fort, S., and Potier, M. C. (2011) Local cholesterol increase triggers amyloid precursor protein-Bace1 clustering in lipid rafts and rapid endocytosis. *FASEB J.* **25**, 295–305
11. Levitan, I., and Barrante, F. J. (2012) Cholesterol Regulation of Ion Channels and Receptors. John Wiley & Sons, Hoboken, NY
12. Fliesler, S. J., and Bretillon, L. (2010) The ins and outs of cholesterol in the vertebrate retina. *J. Lipid Res.* **51**, 3399–3413
13. Brownell, W. E., Jacob, S., Hakizimana, P., Ulfendahl, M., and Fridberger, A. (2011) Membrane cholesterol modulates cochlear electromechanics. *Pflugers Arch.* **461**, 677–686
14. Kacher, R., Lamazière, A., Heck, N., Kappes, V., Mounier, C., Despres, G., Dembitskaya, Y., Perrin, E., Christaller, W., Sasidharan Nair, S., Messent, V., Cartier, N., Vanhoutte, P., Venance, L., Saudou, F., et al. (2019) CYP46A1 gene therapy deciphers the role of brain cholesterol metabolism in Huntington's disease. *Brain* **142**, 2432–2450
15. Jonas, J. B., Aung, T., Bourne, R. R., Bron, A. M., Ritch, R., and Panda-Jonas, S. (2017) Glaucoma. *Lancet* **390**, 2183–2193
16. Križaj, D. (2019) What is glaucoma? In *Webvision: The Organization of the Retina and Visual System*. H. Kolb, E. Fernandez, and R. Nelson, editors. University of Utah Health Sciences Center, Salt Lake City, UT, 1995
17. Choquet, H., Paylakhi, S., Kneeland, S. C., Thai, K. K., Hoffmann, T. J., Yin, J., Kvale, M. N., Banda, Y., Tolman, N. G., Williams, P. A., Schaefer, C., Melles, R. B., Risch, N., John, S. W. M., Nair, K. S., et al. (2018) A multiethnic genome-wide association study of primary open-angle glaucoma identifies novel risk loci. *Nat. Commun.* **9**, 2278
18. Iglesias, A. I., Springelkamp, H., Ramdas, W. D., Klaver, C. C., Willemse, R., and van Duijn, C. M. (2015) Genes, pathways, and animal models in primary open-angle glaucoma. *Eye* **29**, 1285–1298
19. Rao, P. V., Pattabiraman, P. P., and Kopczynski, C. (2017) Role of the Rho GTPase/Rho kinase signaling pathway in pathogenesis and treatment of glaucoma: bench to bedside research. *Exp. Eye Res.* **158**, 23–32
20. Yarishkin, O., Baumann, J. M., and Križaj, D. (2019) Mechanoelectrical transduction in trabecular meshwork involves parallel activation of TRPV4 and TREK-1 channels. *Channels* **13**, 168–171
21. Yarishkin, O., Phuong, T. T. T., Baumann, J. M., de Ieso, M., Vazquez-Chona, F., Rudzitis, C. N., Sundberg, C., Lakk, M., Stamer, D. W., and Križaj, D. (2021) Mechanotransduction and dynamic outflow regulation in trabecular meshwork require Piezol channels. *J. Physiol.* **599**, 571–592
22. Aribindi, K., Guerra, Y., Lee, R. K., and Bhattacharya, S. K. (2013) Comparative phospholipid profiles of control and glaucomatous human trabecular meshwork. *Invest. Ophthalmol. Vis. Sci.* **54**, 3037–3044
23. Vahabikashi, A., Gelman, A., Dong, B., Gong, L., Cha, E. D. K., Schimmel, M., Tamm, E. R., Perkumas, K., Stamer, W. D., Sun, C., Zhang, H. F., Gong, H., and Johnson, M. (2019) Increased stiffness and flow resistance of the inner wall of Schlemm's canal in glaucomatous human eyes. *Proc. Natl. Acad. Sci. U. S. A.* **116**, 26555–26563
24. Pattabiraman, P. P., Rinkoski, T., Poeschla, E., Proia, A., Challa, P., and Rao, P. V. (2015) RhoA GTPase-induced ocular hypertension in a rodent model is associated with increased fibrogenic activity in the trabecular meshwork. *Am. J. Pathol.* **185**, 496–512
25. Tumminia, S. J., Mitton, K. P., Arora, J., Zelenka, P., Epstein, D. L., and Russell, P. (1998) Mechanical stretch alters the actin cytoskeletal network and signal transduction in human trabecular meshwork cells. *Invest. Ophthalmol. Vis. Sci.* **39**, 1361–1371
26. Ryskamp, D. A., Frye, A. M., Phuong, T. T., Yarishkin, O., Jo, A. O., Xu, Y., Lakk, M., Iuso, A., Redmon, S. N., Ambati, B., Hageman, G., Prestwich, G. D., Torrejon, K. Y., and Križaj, D. (2016) TRPV4 regulates calcium homeostasis, cytoskeletal remodeling, conventional outflow and intraocular pressure in the mammalian eye. *Sci. Rep.* **6**, 30583
27. Lakk, M., and Križaj, D. (2021) Mechanoreciprocity requires interactions between TRPV4 channels, the Rho pathway and actin cytoskeleton. *Am. J. Physiol. Cell Physiol.* **320**, C1013–C1030
28. Rocio Servin-Vences, M. R., Moroni, M., Lewin, G. R., and Poole, K. (2017) Direct measurement of TRPV4 and PIEZO1 activity reveals multiple mechanotransduction pathways in chondrocytes. *Elife* **6**, e21074
29. Iuso, A., and Križaj, D. (2016) TRPV4-AQP4 interactions' turbocharge' astroglial sensitivity to small osmotic gradients. *Channels* **10**, 172–174
30. Kumari, S., Kumar, A., Sardar, P., Yadav, M., Majhi, R. K., Kumar, A., and Goswami, C. (2015) Influence of membrane cholesterol in the molecular evolution and functional regulation of TRPV4. *Biochem. Biophys. Res. Commun.* **456**, 312–319
31. Saliez, J., Bouzin, C., Rath, G., Ghisdal, P., Desjardins, F., Rezzani, R., Rodella, L. F., Vriens, J., Nilius, B., Feron, O., Balligand, J. L., and Dessaix, C. (2008) Role of caveolar compartmentation in endothelium-derived hyperpolarizing factor-mediated relaxation: Ca<sup>2+</sup> signals and gap junction function are regulated by caveolin in endothelial cells. *Circulation* **117**, 1065–1074
32. Daneva, Z., Marziano, C., Ottolini, M., Chen, Y. L., Baker, T. M., Kuppusamy, M., Zhang, A., Ta, H. Q., Reagan, C. E., Mihalek, A. D., Kasetti, R. B., Shen, Y., Isakson, B. E., Minshall, R. D., Zode, G. S., et al. (2021) Caveolar peroxynitrite formation impairs

- endothelial TRPV4 channels and elevates pulmonary arterial pressure in pulmonary hypertension. *Proc. Natl. Acad. Sci. U. S. A.* **118**, e2023130118
33. Yarishkin, O., Phuong, T. T. T., Bretz, C. A., Olsen, K. W., Baumann, J. M., Lakk, M., Crandall, A., Heurteaux, C., Hartnett, M. E., and Križaj, D. (2018) TREK-1 channels regulate pressure sensitivity and calcium signaling in trabecular meshwork cells. *J. Gen. Physiol.* **150**, 1660–1675
  34. Grundy, D. (2015) Principles and standards for reporting animal experiments in the journal of physiology and experimental physiology. *J. Physiol.* **593**, 2547–2549
  35. Križaj, D., Gorusupudi, A., Bernstein, P., Toft-Bertelsen, T., Macaulay, N., and Lakk, M. (2020) Cholesterol regulates TRPV4-dependent signaling in the trabecular meshwork. *Invest. Ophthalmol. Vis. Sci.* **61**, 3424
  36. Lakk, M., Toft-Bertelsen, T., Hoffman, G., Gorusupudi, A., Bernstein, P., Macaulay, N., and Križaj, D. (2020) Membrane cholesterol regulates TRPV4 function, cytoskeletal expression and stretch response in trabecular meshwork cells. *bioRxiv*. <https://doi.org/10.1101/2020.12.01.406850>
  37. Zidovetzki, R., and Levitan, I. (2007) Use of cyclodextrins to manipulate plasma membrane cholesterol content: evidence, misconceptions and control strategies. *Biochim. Biophys. Acta* **1768**, 1311–1324
  38. Christian, A. E., Haynes, M. P., Phillips, M. C., and Rothblat, G. H. (1997) Use of cyclodextrins for manipulating cellular cholesterol content. *J. Lipid Res.* **38**, 2264–2272
  39. Romanenko, V. G., Fang, Y., Byfield, F., Travis, A. J., Vandenberg, C. A., Rothblat, G. H., and Levitan, I. (2004) Cholesterol sensitivity and lipid raft targeting of Kir2.1 channels. *Biophys. J.* **87**, 3850–3861
  40. Jo, A. O., Ryskamp, D. A., Phuong, T. T. T., Verkman, A. S., Yarishkin, O., MacAulay, N., and Križaj, D. (2015) TRPV4 and AQP4 channels synergistically regulate cell volume and calcium homeostasis in retinal Müller glia. *J. Neurosci.* **35**, 13525–13537
  41. Toft-Bertelsen, T. L., Yarishkin, O., Redmon, S., Phuong, T. T. T., Križaj, D., and MacAulay, N. (2019) Volume sensing in the transient receptor potential vanilloid 4 ion channel is cell type-specific and mediated by an N-terminal volume-sensing domain. *J. Biol. Chem.* **294**, 18421–18434
  42. Folch, J., Lees, M., and Stanley, G. H. (1957) A simple method for the isolation and purification of total lipides from animal tissues. *J. Biol. Chem.* **226**, 497–509
  43. Lakk, M., Young, D., Baumann, J. M., Jo, A. O., Hu, H., and Križaj, D. (2018) Polymodal TRPV1 and TRPV4 sensors colocalize but do not functionally interact in a subpopulation of mouse retinal ganglion cells. *Front. Cell. Neurosci.* **12**, 353
  44. Ryskamp, D. A., Witkovsky, P., Barabas, P., Huang, W., Koehler, C., Akimov, N. P., Lee, S. H., Chauhan, S., Xing, W., Rentería, R. C., Liedtke, W., and Krizaj, D. (2011) The polymodal ion channel transient receptor potential vanilloid 4 modulates calcium flux, spiking rate, and apoptosis of mouse retinal ganglion cells. *J. Neurosci.* **31**, 7089–7101
  45. Lakk, M., Yarishkin, O., Baumann, J. M., Iuso, A., and Križaj, D. (2017) Cholesterol regulates polymodal sensory transduction in Müller glia. *Glia* **65**, 2038–2050
  46. Ryskamp, D. A., Jo, A. O., Frye, A. M., Vazquez-Chona, F., MacAulay, N., Thoreson, W. B., and Križaj, D. (2014) Swelling and eicosanoid metabolites differentially gate TRPV4 channels in retinal neurons and glia. *J. Neurosci.* **34**, 15689–156700
  47. Molnar, T., Barabas, P., Birnbaumer, L., Punzo, C., Kefalov, V., and Križaj, D. (2012) Store-operated channels regulate intracellular calcium in mammalian rods. *J. Physiol.* **590**, 3465–3481
  48. Toft-Bertelsen, T. L., Križaj, D., and MacAulay, N. (2017) When size matters: transient receptor potential vanilloid 4 channel as a volume-sensor rather than an osmo-sensor. *J. Physiol.* **595**, 3287–3302
  49. Fenton, R. A., Moeller, H. B., Zelenina, M., Snaebjornsson, M. T., Holen, T., and MacAulay, N. (2010) Differential water permeability and regulation of three aquaporin 4 isoforms. *Cell. Mol. Life Sci.* **67**, 829–840
  50. Bratengeier, C., Liszka, A., Hoffman, J., Bakker, A. D., and Fahlgren, A. (2020) High shear stress amplitude in combination with prolonged stimulus duration determine induction of osteoclast formation by hematopoietic progenitor cells. *FASEB J.* **34**, 3755–3772
  51. Gimpl, G., and Gehrig-Burger, K. (2011) Probes for studying cholesterol binding and cell biology. *Steroids* **76**, 216–231
  52. Wei, H., Malcor, J. M., and Harper, M. T. (2018) Lipid rafts are essential for release of phosphatidylserine-exposing extracellular vesicles from platelets. *Sci. Rep.* **8**, 9987
  53. Strotmann, R., Harteneck, C., Nunnenmacher, K., Schultz, G., and Plant, T. D. (2000) OTRPC4, a non-selective cation channel that confers sensitivity to extracellular osmolarity. *Nat. Cell Biol.* **2**, 695–702
  54. Liedtke, W., Choe, Y., Martí-Renom, M. A., Bell, A. M., Denis, C. S., Sali, A., Hudspeth, A. J., Friedman, J. M., and Heller, S. V. (2000) Vanilloid receptor-related osmotically activated channel (VR-OAC), a candidate vertebrate osmoreceptor. *Cell* **103**, 525–535
  55. Jo, A. O., Lakk, M., Frye, A. M., Phuong, T. T. T., Redmon, S. N., Roberts, R., Berkowitz, B. A., Yarishkin, O., and Križaj, D. (2016) Differential volume regulation and calcium signaling in two ciliary body cell types is subserved by TRPV4 channels. *Proc. Natl. Acad. Sci. U. S. A.* **113**, 3885–3890
  56. Phuong, T. T. T., Redmon, S. N., Yarishkin, O., Winter, J. M., Li, D. Y., and Križaj, D. (2017) Calcium influx through TRPV4 channels modulates the adherens contacts between retinal microvascular endothelial cells. *J. Physiol.* **595**, 6869–6885
  57. Lapajne, L., Lakk, M., Yarishkin, O., Gubeljak, L., Hawlina, M., and Križaj, D. (2020) Polymodal sensory transduction in mouse corneal epithelial cells. *Invest. Ophthalmol. Vis. Sci.* **61**, 2
  58. White, J. P., Cibelli, M., Urban, L., Nilius, B., McGeown, J. G., and Nagy, I. (2016) TRPV4: molecular conductor of a diverse orchestra. *Physiol. Rev.* **96**, 911–973
  59. Grierson, I., and Lee, W. R. (1975) Pressure-induced changes in the ultrastructure of the endothelium lining Schlemm's canal. *Am. J. Ophthalmol.* **80**, 863–884
  60. Johnstone, M. A. (2004) The aqueous outflow system as a mechanical pump: evidence from examination of tissue and aqueous movement in human and non-human primates. *J. Glaucoma* **13**, 421–438
  61. Sherwood, J. M., Stamer, W. D., and Overby, D. R. (2019) A model of the oscillatory mechanical forces in the conventional outflow pathway. *J. R. Soc. Interface* **16**, 20180652
  62. Chubinskij-Nadezhdin, V. I., Efremova, T. N., Khaitlina, S. Y., and Morachevskaia, E. A. (2013) Functional impact of cholesterol sequestration on actin cytoskeleton in normal and transformed fibroblasts. *Cell. Biol. Int.* **37**, 617–623
  63. Morenilla-Palao, C., Pertusa, M., Meseguer, V., Cabedo, H., and Viana, F. (2009) Lipid raft segregation modulates TRPM8 channel activity. *J. Biol. Chem.* **284**, 9215–9224
  64. Naylor, J., Li, J., Milligan, C. J., Zeng, F., Sukumar, P., Hou, B., Sedom, A., Yuldasheva, N., Majeed, Y., Beri, D., Jiang, S., Seymour, V. A., McKeown, L., Kumar, B., Harteneck, C., et al. (2010) Pregnanolone sulphate- and cholesterol-regulated TRPM3 channels coupled to vascular smooth muscle secretion and contraction. *Circ. Res.* **106**, 1507–1515
  65. Picazo-Juárez, G., Romero-Suárez, S., Nieto-Posadas, A., Llorente, I., Jara-Osegueda, A., Briggs, M., McIntosh, T. J., Simon, S. A., Ladron-de-Guevara, E., Islas, L. D., and Rosenbaum, T. (2011) Identification of a binding motif in the S5 helix that confers cholesterol sensitivity to the TRPV1 ion channel. *J. Biol. Chem.* **286**, 24966–24976
  66. Berna-Erro, A., Izquierdo-Serra, M., Sepúlveda, R. V., Rubio-Moscardo, F., Doñate-Macián, P., Serra, S. A., Carrillo-García, J., Péralvarez-Marín, A., González-Nilo, F., Fernández-Fernández, J. M., and Valverde, M. A. (2017) Structural determinants of 5,6'-epoxyeicosatrienoic acid binding to and activation of TRPV4 channel. *Sci. Rep.* **7**, 10522
  67. Redmon, S. N., Shibasaki, K., and Križaj, D. (2016) Transient receptor potential cation channel subfamily V member 4 (TRPV4). In *Encyclopedia of Signaling Molecules*. S. Choi, editor. Springer Nature, New York, NY
  68. Santiago, J., Guzmán, G. R., Rojas, L. V., Martí, R., Asmar-Rovira, G. A., Santana, L. F., McNamee, M., and Lasalde-Dominicci, J. A. (2001) Probing the effects of membrane cholesterol in the *Torpedo californica* acetylcholine receptor and the novel lipid-exposed mutation alpha C418W in *Xenopus* oocytes. *J. Biol. Chem.* **276**, 46523–46532
  69. Liedtke, W., and Friedman, J. M. (2003) Abnormal osmotic regulation in trpv4-/- mice. *Proc. Natl. Acad. Sci. U. S. A.* **100**, 13698–13703

70. Zhao, Y., Huang, H., Jiang, Y., Wei, H., Liu, P., Wang, W., and Niu, W. (2012) Unusual localization and translocation of TRPV4 protein in cultured ventricular myocytes of the neonatal rat. *Eur. J. Histochem.* **56**, e32
71. Hochstetler, A. E., Smith, H. M., Preston, D. C., Reed, M. M., Territo, P. R., Shim, J. W., Fulkerson, D., and Blazer-Yost, B. L. (2020) TRPV4 antagonists ameliorate ventriculomegaly in a rat model of hydrocephalus. *JCI Insight*. **5**, e137646
72. Fielding, C. J., and Fielding, P. E. (2000) Cholesterol and caveolae: structural and functional relationships. *Biochim. Biophys. Acta*. **1529**, 210–222
73. Ridone, P., Pandzic, E., Vassalli, M., Cox, C. D., Macmillan, A., Gottlieb, P. A., and Martinac, B. (2020) Disruption of membrane cholesterol organization impairs the activity of PIEZO1 channel clusters. *J. Gen. Physiol.* **152**, e201912515
74. Saha, S., Ghosh, A., Tiwari, N., Kumar, A., Kumar, A., and Goswami, C. (2017) Preferential selection of arginine at the lipid-water-interface of TRPV1 during vertebrate evolution correlates with its snorkeling behaviour and cholesterol interaction. *Sci. Rep.* **7**, 16808
75. Balsle, E., El-Haou, S., Dillanian, G., Dauphin, A., Eldstrom, J., Fedida, F., Coulombe, A., and Hatem, S. N. (2009) Cholesterol modulates the recruitment of Kv1.5 channels from Rab11-associated recycling endosome in native atrial myocytes. *Proc. Natl. Acad. Sci. U. S. A.* **106**, 14681–14686
76. Levitan, I., Christian, A. E., Tuleko, T. N., and Rothblat, G. H. (2000) Membrane cholesterol content modulates activation of volume-regulated anion current in bovine endothelial cells. *J. Gen. Physiol.* **115**, 405–416
77. Graziani, A., Bricko, V., Carmignani, M., Graier, W. F., and Groschner, K. (2004) Cholesterol- and caveolin-rich membrane domains are essential for phospholipase A2-dependent EDHF formation. *Cardiovasc. Res.* **64**, 234–242
78. Rodal, S. K., Skretting, G., Garred, O., Vilhardt, F., van Deurs, B., and Sandvig, K. (1999) Extraction of cholesterol with methyl-beta-cyclodextrin perturbs formation of clathrin-coated endocytic vesicles. *Mol. Biol. Cell*. **10**, 961–974
79. Zhang, Y., Daday, C., Gu, R. X., Cox, C. D., Martinac, B., de Groot, B. L., and Walz, T. (2021) Visualization of the mechanosensitive ion channel MscS under membrane tension. *Nature*. **590**, 509–514
80. Teng, J., Loukin, S. H., Anishkin, A., and Kung, C. (2015) L596-W733 bond between the start of the S4-S5 linker and the TRP box stabilizes the closed state of TRPV4 channel. *Proc. Natl. Acad. Sci. U. S. A.* **112**, 3386–3391
81. Perozo, E., Kłoda, A., Cortes, D. M., and Martinac, B. (2002) Physical principles underlying the transduction of bilayer deformation forces during mechanosensitive channel gating. *Nat. Struct. Biol.* **9**, 696–703
82. Anishkin, A., Loukin, S. H., Teng, J., and Kung, C. (2013) Stiffened lipid platforms at molecular force foci. *Proc. Natl. Acad. Sci. U. S. A.* **110**, 4886–4892
83. Bukiya, A. N., Belani, J. D., Rychnovsky, S., and Dopico, A. M. (2011) Specificity of cholesterol and analogs to modulate B.K. channels points to direct sterol-channel protein interactions. *J. Gen. Physiol.* **137**, 93–110
84. Lei, L., Lu, S., Wang, Y., Kim, T., Mehta, D., and Wang, Y. (2014) The role of mechanical tension on lipid raft dependent PDGF-induced TRPC6 activation. *Biomaterials*. **35**, 2868–2877
85. Lockwich, T. P., Liu, X., Singh, B. B., Jadlowiec, J., Weiland, S., and Ambudkar, I. S. (2000) Assembly of Trpl in a signaling complex associated with caveolin-scaffolding lipid raft domains. *J. Biol. Chem.* **275**, 11934–11942
86. Sághy, É., Szőke, É., Payrits, M., Helyes, Z., Börzsei, R., Erostýák, J., Jánosi, T. Z., Sétáló, G., and Szolcsányi, J. (2015) Evidence for the role of lipid rafts and sphingomyelin in Ca<sup>2+</sup>-gating of transient receptor potential channels in trigeminal sensory neurons and peripheral nerve terminals. *Pharmacol. Res.* **100**, 101–116
87. Peters, M., Katz, B., Lev, S., Zaguri, R., Gutorov, R., and Minke, B. (2017) Depletion of membrane cholesterol suppresses drosophila transient receptor potential-like (TRPL) channel activity. *Curr. Top. Membr.* **80**, 233–254
88. Startek, J. B., Boonen, B., López-Requena, A., Talavera, A., Alpizar, Y. A., Ghosh, D., Van Ranst, N., Nilius, B., Voets, T., and Talavera, K. (2019) Mouse TRPA1 function and membrane localization are modulated by direct interactions with cholesterol. *Elife*. **8**, e46084
89. Klausen, T. K., Janssens, A., Prenen, J., Owsianik, G., Hoffmann, E. K., Pedersen, S. F., and Nilius, B. (2014) Single point mutations of aromatic residues in transmembrane helices 5 and -6 differentially affect TRPV4 activation by 4 $\alpha$ -PDD and hypotonicity: implications for the role of the pore region in regulating TRPV4 activity. *Cell Calcium*. **55**, 38–47
90. Das, R., and Goswami, C. (2019) TRPV4 expresses in bone cell lineages and TRPV4-R616Q mutant causing Brachyolmia in human reveals “loss-of-interaction” with cholesterol. *Biochem. Biophys. Res. Commun.* **517**, 566–574
91. Loukin, S. H., Su, Z., and Kung, C. (2009) Hypotonic shocks activate rat TRPV4 in yeast in the absence of polyunsaturated fatty acids. *FEBS Lett.* **583**, 754–758
92. Liu, M., Huang, W., Wu, D., and Priestley, J. V. (2006) TRPV1, but not P2X<sub>3</sub>, requires cholesterol for its function and membrane expression in rat nociceptors. *Eur. J. Neurosci.* **24**, 1–6
93. Szoke, E., Börzsei, R., Tóth, D. M., Lengl, O., Helyes, Z., Sándor, Z., and Szolcsányi, J. (2010) Effect of lipid raft disruption on TRPV1 receptor activation of trigeminal sensory neurons and transfected cell line. *Eur. J. Pharmacol.* **628**, 67–74
94. Klausen, T. K., Hougaard, C., Hoffmann, E. K., and Pedersen, S. F. (2006) Cholesterol modulates the volume-regulated anion current in Ehrlich-Lettre ascites cells via effects on Rho and F-actin. *Am. J. Physiol. Cell Physiol.* **291**, C757–C771
95. Hissa, B., Oakes, P. W., Pontes, B., Juan, G. R-S., and Gardel, M. L. (2017) Cholesterol depletion impairs contractile machinery in neonatal rat cardiomyocytes. *Sci. Rep.* **7**, 43764
96. Goswami, C., Kuhn, J., Heppenstall, P. A., and Hucho, T. (2010) Importance of non-selective cation channel TRPV4 interaction with cytoskeleton and their reciprocal regulations in cultured cells. *PLoS One*. **5**, e11654
97. Oesterle, A., Laufs, U., and Liao, J. K. (2017) Pleiotropic effects of statins on the cardiovascular system. *Circ. Res.* **120**, 229–243
98. Bradley, J. M., Kelley, M. J., Zhu, X., Andersohn, A. M., Alexander, J. P., and Acott, T. S. (2001) Effects of mechanical stretching on trabecular matrix metalloproteinases. *Invest. Ophthalmol. Vis. Sci.* **42**, 1505–1513
99. Borrás, T. (2003) Gene expression in the trabecular meshwork and the influence of intraocular pressure. *Prog. Retin. Eye Res.* **22**, 435–463
100. Yarishkin, O., Phuong, T. T. T., Baumann, J. M., De Ieso, M. L., Vazquez-Chona, F., Rudzitis, C. N., Sundberg, C., Lakk, M., Stamer, W. D., and Križaj, D. (2021) Piezol channels mediate trabecular meshwork mechanotransduction and promote aqueous fluid outflow. *J. Physiol.* **599**, 571–592
101. Carreon, T. A., Castellanos, A., Gasull, X., and Bhattacharya, S. K. (2017) Interaction of cochlin and mechanosensitive channel TREK-1 in trabecular meshwork cells influences the regulation of intraocular pressure. *Sci. Rep.* **7**, 452
102. Filla, M. S., Faralli, J. A., Desikan, H., Peotter, J. L., Wannow, A. C., and Peters, D. M. (2019) Activation of  $\alpha\beta\beta$  integrin alters fibronectin fibril formation in human trabecular meshwork cells in a ROCK-independent manner. *Invest. Ophthalmol. Vis. Sci.* **60**, 3897–3913
103. Zhu, W., Hou, F., Fang, J., Bahrami Fard, M. R., Liu, Y., Ren, S., Wu, S., Qi, Y., Sui, S., Read, A. T., Sherwood, J. M., Zou, W., Yu, H., Zhang, J., Overby, D. R., et al. (2021) The role of Piezol in conventional aqueous humor outflow dynamics. *iScience*. **24**, 102042
104. Elliott, M. H., Ashpole, N. E., Gu, X., Herrnberger, L., McClellan, M. E., Griffith, G. L., Reagan, A. M., Boyce, T. M., Tanito, M., Tamm, E. R., and Stamer, W. D. (2016) Caveolin-1 modulates intraocular pressure: implications for caveolae mechanoprotection in glaucoma. *Sci. Rep.* **6**, 37127
105. Kizhatil, K., Chlebowski, A., Tolman, N. G., Freeburg, N. F., Ryan, M. M., Shaw, N. N., Kokini, A. D., Marchant, J. K., and John, S. W. (2016) An in vitro perfusion system to enhance outflow studies in mouse eyes. *Invest. Ophthalmol. Vis. Sci.* **57**, 5207–5215
106. De Ieso, M. L., Gurley, J. M., McClellan, M. E., Gu, X., Navarro, I., Li, G., Gomez-Caraballo, M., Enyong, E., Stamer, W. D., and Elliott, M. H. (2020) Physiologic consequences of caveolin-1 ablation in conventional outflow endothelia. *Invest. Ophthalmol. Vis. Sci.* **61**, 32
107. Butenko, O., Dzamba, D., Benesova, J., Honsa, P., Benfenati, V., Rusnakova, V., Ferroni, S., and Anderova, M. (2012) The increased activity of TRPV4 channel in the astrocytes of the adult rat hippocampus after cerebral hypoxia/ischemia. *PLoS One*. **7**, e39959